

Brock University



Physics Department

St. Catharines, Ontario, Canada L2S 3A1

PHYS 5P80 Laboratory Manual

Physics Department

Copyright © Brock University, 2020–2021

Contents

1	Preparation of a thin Bi film by vacuum evaporation	1
1.1	Introduction	1
1.2	Sample preparation checklists	6
1.3	Measuring film thickness	7
2	Resistivity and Hall effect in a thin bismuth film	11
2.1	Introduction	11
2.2	Measurement checklists	13
3	Gamma-ray scintillation spectroscopy and the Compton effect	17
3.1	The scintillation spectrometer	17
3.2	The Compton effect	21
4	Energy-dispersive X-ray diffraction	25
4.1	Introduction	25
4.2	The apparatus	26
4.3	Measurement checklist	30
5	Electron Diffraction	33
5.1	Introduction	33
5.2	The apparatus	35
5.3	Measurement checklist	36
6	The photoelectric effect	39
6.1	Introduction	39
6.2	The apparatus	39
6.3	Measurement checklist	43
7	Blackbody radiation spectra	45
7.1	Introduction	45
7.2	The apparatus	47
7.3	Measurement checklist	48
8	Raman spectroscopy	49
8.1	Introduction	49
8.2	The apparatus	49
8.3	Measurement checklist	52

Experiment 1

Preparation of a thin Bi film by vacuum evaporation

Basics of vacuum technology (pumps, valves, gauges) and vacuum evaporation techniques are explored in this experiment. Some of the equipment in use is dangerous and delicate; if unsure of how to proceed safely (for yourself or the equipment) be sure to consult the instructor first.

1.1 Introduction

Thin layers (“films”) of solid materials, with thickness $\simeq 10^{-6}\text{m}$, are important components of many modern electronic and optical devices. They are often produced by evaporating the material in a vacuum and condensing the vapor on a substrate until the desired thickness is reached. Modern techniques of molecular beam epitaxy are far more elaborate than our simple experimental setup, but the fundamental principles are the same.

Deposition is done in vacuum in order to:

- prevent a chemical reaction of the material with atmospheric gases;
- lower the boiling/sublimation temperature; and,
- deposit the material in a smooth, even manner on the substrate.

In this experiment you will produce a thin film of Bismuth on a glass substrate, and measure its thickness with a Michelson interferometer. The electrical properties of the film will be investigated in a subsequent experiment.

Outline of the evaporator operation

To perform *vacuum* evaporation, the evaporator’s bell jar needs to be *evacuated* first, using a two-stage pumping station. Schematically the setup is shown in Fig. 1.1, showing two different regimes of pumping: roughing and high-vacuum modes. Be sure to read the following section very carefully. Operation of high-vacuum equipment has special safety considerations for the user, and failure to adhere to the proper procedure may result in catastrophic failures of expensive equipment.

The roughing regime is using a mechanical pump to evacuate the bell jar, via the bypass, to a pressure of about $\simeq 10$ mTorr. The evacuated gas is ejected into the room air, and since the back-flow is prevented by bubbling the gas through the pump oil, a fine oil mist is sometimes generated; the filter on the output of the mechanical “roughing” pump catches that oil. During this regime, a significant bubbling noise is heard, but it quickly diminishes as the pressure begins to decrease. If it does not, and the pump continues to be noisy, there is a leak: check that the bell jar vent valve is closed, that the bell jar itself is making a firm seal with the base plate, and that the transfer lines are all secured. If the turbo pump is already spinning, it must be completely isolated from the roughing pathway and maintained at low pressure. This initial evacuation of a bell jar to about 10 mTorr usually takes about 10 minutes. During the roughing regime, the gas pressure is too high for either ion gauge or the cold-cathode pressure gauges, and must be monitored only through the thermocouple (TC) gauge. The cold cathode gauge can be in stand-by mode

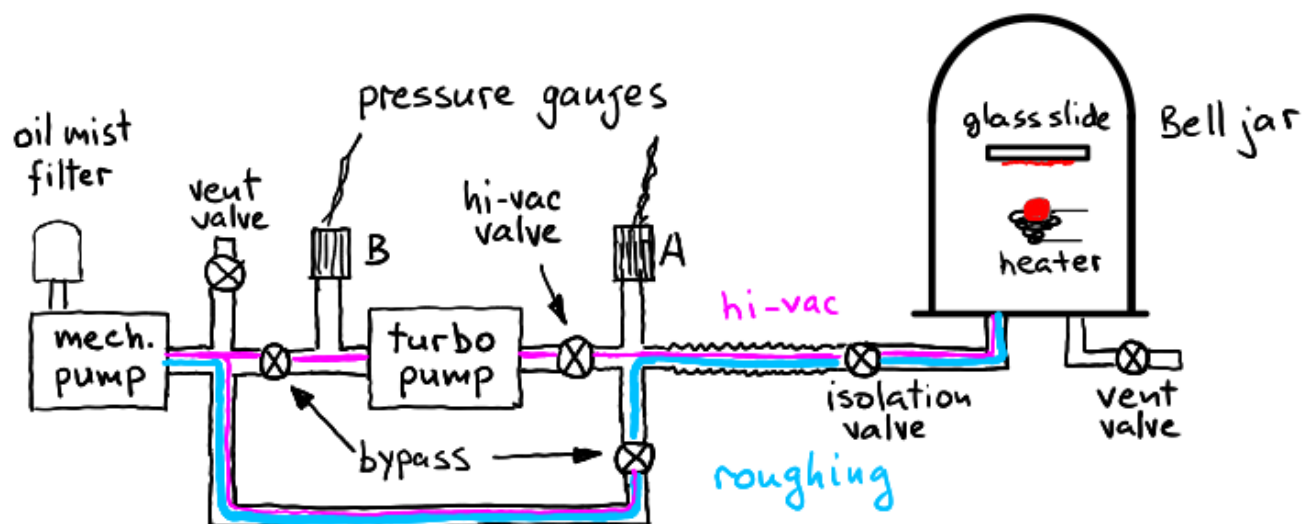


Figure 1.1: Schematic diagram of the evaporator setup, showing two different regimes of pumping: roughing and high-vacuum modes.

(high voltage off). At the completion of the roughing process, both TC gauges A and B should show the same pressure of about 10 mTorr.

After the pressure is lowered sufficiently for the safe operation of the turbo pump, the bypass pathway can be closed and the mechanical pump switched to the back-end support of the turbo pump. If the turbo pump was already spinning, isolated, the bypass valve connecting mechanical and turbo pump can now be slowly opened, followed by a slow opening of the hi-vac valve, completing the switchover to the hi-vac pumping pathway. At no time should the turbo pump be asked to pump at its front inlet without first establishing a back-end support from a mechanical pump.

Once in the hi-vac regime, the turbo pump can pump down to $\simeq 10^{-5}$ – 10^{-6} Torr. The ion or cold-cathode gauge can be safely operated below a few mTorr, and there should be some difference in pressure between the front and back ends of the turbo pump (TC A and TC B readings will differ); this indicates that the turbo pump is working. As the pumping continues, this difference will become smaller and will disappear when high vacuum is reached, as shown in Fig. 1.2. If the pressure fails to reach $\simeq 10^{-5}$ Torr after about 10-15 minutes of hi-vac operation, check for leaks: tighten the connectors and vent valves. If a rubber seal on the bell jar is suspected, immediately isolate the turbo pump, turn off the cold-cathode gauge, and switch to the roughing pathway, before trying to adjust the rubber seal. A sudden exposure to room pressure will cause a catastrophic failure of the turbo pump.

The evaporation takes place in a glass bell jar, when a tungsten filament coiled up into a small crucible is heated; it acts as a boiling reservoir for a small quantity of bismuth. Bismuth vapour then condenses on a nearby surface of a clean glass substrate (a microscope slide), held in a custom frame directly above the crucible. The film is deposited on the downward-facing side of the glass slide, usually through a mask of the desired shape sandwiched onto the slide. The best way to monitor the deposition process is to find a line of sight that passes through the glass slide and the opening in the mask to the crucible, then slowly increase the current to the crucible until it begins to glow red, and quickly turn off the crucible current when the view of the crucible through the opening in the mask grows dim, obscured by a bismuth film being formed on the glass. The arrangement can be seen in Fig. 1.3. The length of time for the deposition process should be monitored and recorded, to ensure a correction can be made on the next attempt, if the film turns out to be too thin or too thick.

Bismuth vapour also condenses on the inside of the bell jar, necessitating a thorough cleaning of the

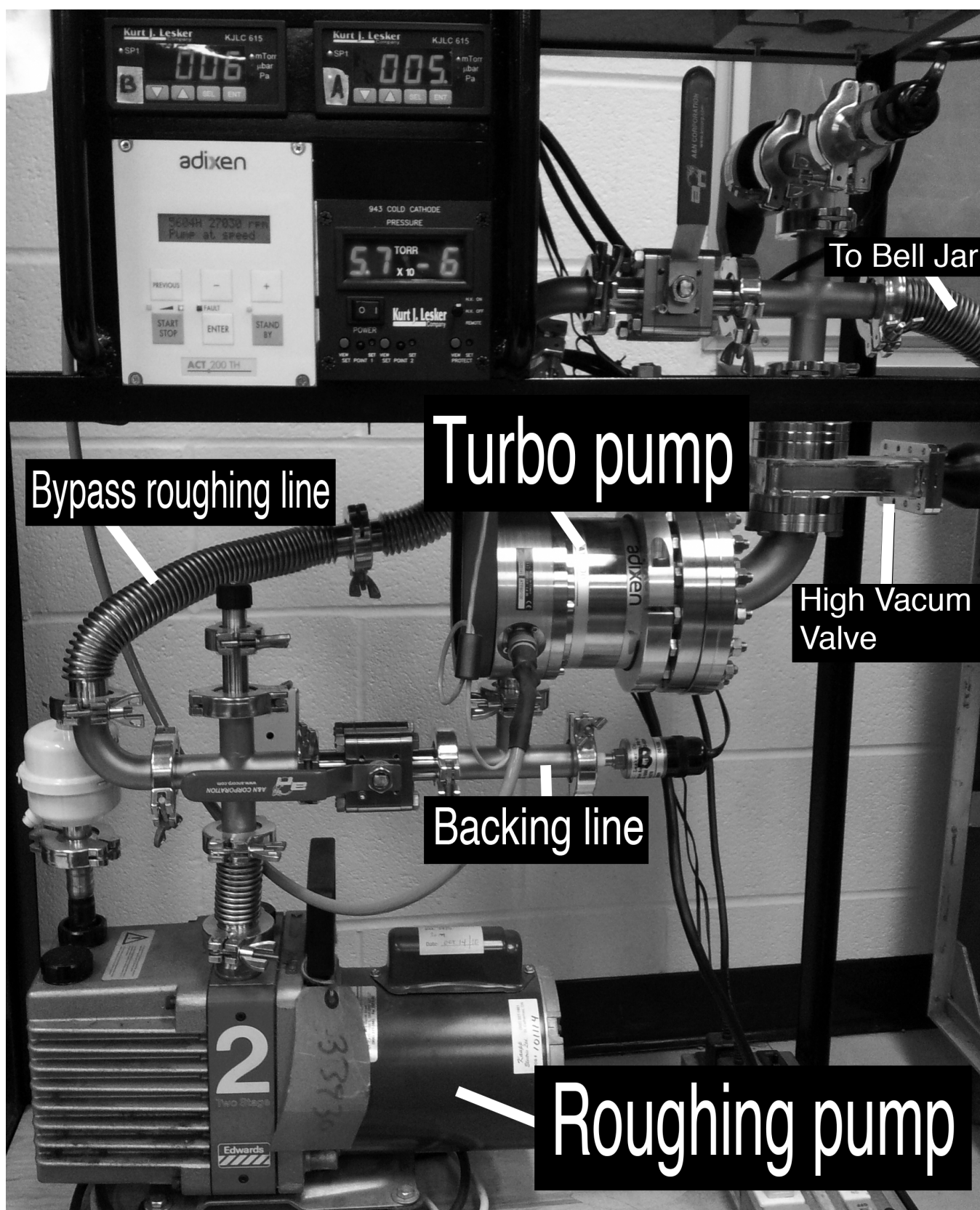


Figure 1.2: The pumping station, showing various TC and cold-cathod gauges, and the control panel of the turbo pump at the top left.



Figure 1.3: The tungsten crucible glows red, melting a small pellet of Bi metal placed into it. The glass slide with a mask plate underneath it is seen directly above the crucible. The score mark on the top surface of the glass slide is visible; the slide can be split into two separate samples along this mark.

inside of the bell jar between preparations.

Once the deposition has occurred, high-vac and the isolation valves can be closed and the bell jar slowly¹ filled with air through its vent valve, after which the bell jar can be lifted and placed sideways on foam supports for cleaning, and the sample extracted. Be sure to remove the deposition mask from the slide without sliding it sideways, to avoid scratching the newly made sample. During this time the turbo pump can continue to run, to maintain low pressure in the pumping system, but it must be isolated before the bell jar is reassembled, its vent valve closed, and the pumping station switched again to the roughing regime, to repeat the evaporation cycle.

At the end of operations, pumps need to be turned off. Consult the instructor: if another group still needs to perform their experiment, the instructor may recommend that the pumping continues overnight. To shut down the pumping system safely, the turbo pump can be isolated with bypass and hi-vac valves, and switch into spin-down mode on the control panel. This will take several minutes to complete. The turbo pump can be left under whatever high-vacuum remains inside it when it is not operating, but once the mechanical pump is turned off, the space in front of it must be vented to the atmosphere through its own vent valve. If this is not done, the vacuum there will suck the pump oil into the piping of the vacuum system, requiring a long and laborious cleanup.

Film thickness

Good films can be produced when the atoms/molecules of the material, in our case Bi, travel from the hot filament to the substrate directly, without colliding with residual air molecules, and when the substrate is clean and has no impurities on its surface. In this respect the following parameters are important and can be calculated from the kinetic theory of gases:

1. The number density of gas N_0 ; which is the number of gas molecules per unit volume, can be calculated from the ideal gas law as

$$N_0 = \frac{P}{kT} \quad (1.1)$$

where P is pressure, T is temperature, and $k = 1.38 \times 10^{-23} \text{JK}^{-1}$ is the Boltzmann constant.

2. The average speed \bar{V} of the gas molecules can be found from

$$\bar{V} = \sqrt{\frac{8kT}{\pi m}} \quad (1.2)$$

where m = mass of the gas molecule.

3. The mean free path \bar{L} of the molecules is given by

$$\bar{L} = \frac{1}{\sqrt{2}\pi d^2 N_0} \quad (1.3)$$

where d is the diameter of molecule.

4. The rate at which gas molecules collide with a surface (collisions per unit per unit time) can be found from

$$\mu = \frac{1}{4} N_0 \bar{V}. \quad (1.4)$$

¹Why slowly? be sure to understand the answer to this question before proceeding.

Exercise

Calculate and plot versus as a function of pressure P , the quantities N_0 , \bar{V} , \bar{L} and μ for $P = 760$ Torr, 76 Torr, *etc.*, down to 7.6×10^{-6} Torr. Use nitrogen at room temperature as the gas: $d = 3.73 \times 10^{-10}$ m. Use double logarithmic scales for your graph.

At what values of P and T are the following conditions met:

1. \bar{L} is approximately equal to the distance from boiling reservoir to the substrate ($\simeq 10$ cm) ?
2. The collision rate $(\text{m}^2\text{s})^{-1}$ about equal to the typical numbers of atoms per m^2 of substrate surface ($\simeq 3 \times 10^{19} \text{m}^{-2}$) ?

It should be clear from your calculations that a vacuum of $< 10^{-4}$ Torr is required for proper vacuum evaporation.

1.2 Sample preparation checklists

Use the vacuum evaporator to produce a thin film of Bi, circular in shape, with four contact pads suitable for making electrical measurements. If in doubt, contact the instructor first.

Preparation of substrate for film deposition

These steps remove water and grease from the microscope slide. Ethanol may dissolve grease from your fingers and leave it on the glass when it evaporates. Use gloves.

1. Score the slide down the middle so that the slide may be split in two.
2. Wash the glass slide with detergent and water.
3. Rinse with distilled water.
4. Rinse with ethanol.
5. Dry the slide in air. Check that it is clean.

Deposition of the bismuth film

1. Check that the ion or cold-cathode gauge is off.
2. Close the high vacuum valve, the by-pass roughing line, and the isolation valve which connects the bell jar to the pumps.
3. Vent the vacuum chamber by opening the vent valve, and lift the bell jar.
4. Put some bismuth into the filament basket.
5. Place the mask on top of the clean slide (on the opposite side of the score mark), and place it, mask side down, into the holder frame. Center the opening in the mask 5-10 cm above the crucible.
6. Clean the inside of the bell jar, especially near the top so that you can look inside. Put the bell jar back on; make sure that the vent valve is closed.
7. Switch the pumping station into the roughing regime. If the turbo pump is spinning, it can remain spinning provided it is isolated on both sides by the hi-vac and roughing valves. Open the valves in-between the roughing pump and the bell jar. Use the roughing pump and pump down the bell jar to about 10-20 mTorr via the roughing bypass.

8. Close the bypass valve on the high-vacuum side, and open the valve connecting the mechanical pump and the turbo pump. Slowly open the high vacuum gate valve. The turbo pump will now start removing the “low pressure” residual air from the bell jar. After a few minutes the pressure should fall below 10^{-4} Torr and the cold-cathode gauge can be switched on. Wait until the pressure is $\leq 5 \times 10^{-5}$ Torr before starting the evaporation. This may take up to 20 minutes.
9. Turn on the filament supply switch, increase the current slowly from zero until the filament just starts glowing. Keep it like that for a minute to outgas it. Increase filament current, until bismuth melts and starts evaporating. Hold filament current until you can no longer see the glow from the top of the bell jar through the opening in the mask and much of Bi has evaporated, as seen from the side.
10. Dial down the current, and turn off the current supply.
11. Repeat steps 1. – 3.
12. Remove slide with bismuth film on it, lift the mask straight up without dragging sideways.
13. Reassemble a fresh glass slide-and-mask “sandwich”, place it in the holding frame, mask side down, replenish Bi in the crucible, replace the bell jar, and start evacuating the evaporator chamber to high vacuum again, in preparation of the next sample, or for the next group of students.

1.3 Measuring film thickness

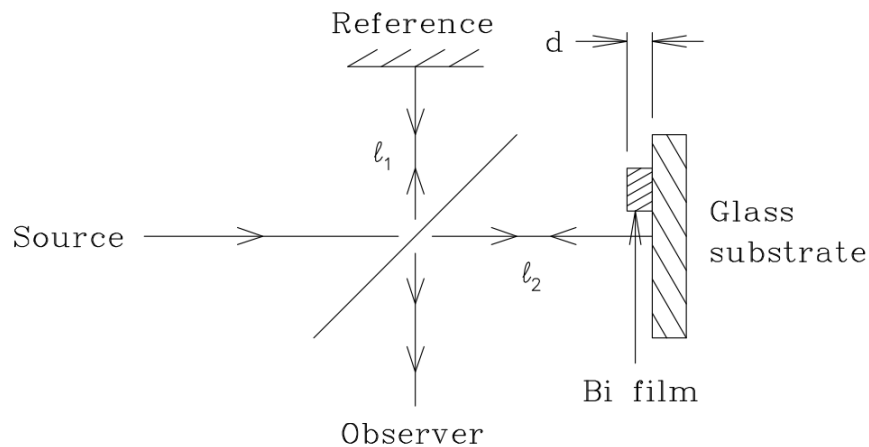


Figure 1.4: A schematic diagram of a Michelson Interferometer.

Since the film thickness d is of the same order of magnitude as the wavelength of visible light, we will use a device that uses interference of light waves to measure the thickness of the film, the Michelson Interferometer, as illustrated in the schematic diagram of Fig. 1.4. When the optical paths ℓ_1 and ℓ_2 differ by $k\lambda$ ($k = 0, 1, 2, \dots$) the monochromatic waves of wavelength λ are reflected back to the observer out of phase, and destructive interference produces a pattern of fringes in the field of view. The spacing between fringes varies, and depends on the angle of slight misalignment of the reflecting plane from being perpendicular to the optical axis. minute adjustments can create a convenient regular grid of fringe lines of certain spacing.

The glass substrate with a thin metal film on it form one mirror of the interferometer. The light reflecting from the Bi film travels a distance $2d$ less than the light reflected from the glass slide, and therefore the fringe pattern over the Bi film shifts with respect to the pattern over the glass slide. From the amount of shift, in units of the fringe spacing, the thickness d can be easily calculated.

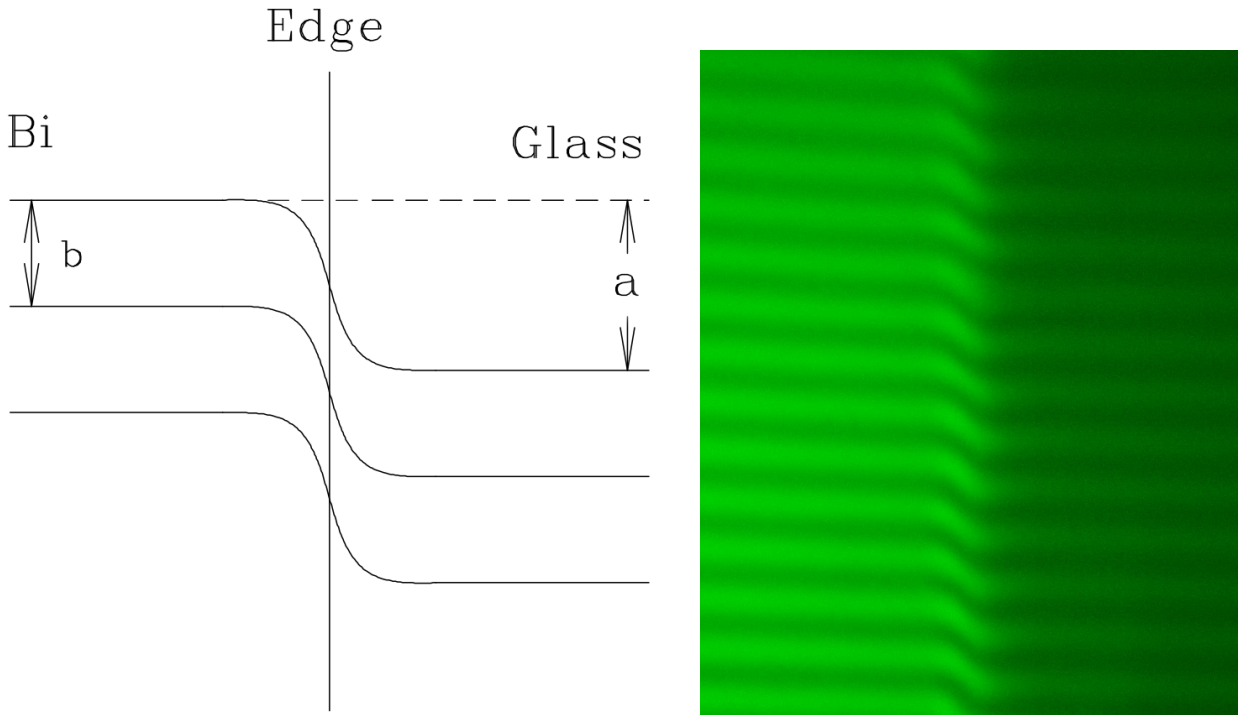


Figure 1.5: A shift in the fringe pattern can be used to find film thickness as $d = \frac{a}{b} \times \frac{\lambda}{2}$. A typical image is on the right, a schematic illustration of how to measure a and b is on the left.

The actual instrument is a Michelson interferometer optically "folded-up" so that it fits over a microscope ($\times 10$) objective. It contains the beam splitter and reference mirror (which can be tilted) and a means of controlling the distance ℓ_1 .

Thickness measurement checklist

Put the sample under a microscope, Bi-film-side up, and check the uniformity of the film, by measuring its thickness at several points all around the periphery of the sample.

1. The instructor will have put the interferometer over the microscope objective, and adjust ℓ_1 until a clear fring pattern is seen. Be careful not to disturb the alignment.
2. Place your slide (film up) under the microscope; turn the backlight illumination on; use white light.
3. Focus on a film edge by adjusting the vertical position of the microscope stage. This sets the distance ℓ_2 .
4. Turn off the backlight, and switch to monochromatic top illumination by putting a Fabry-Perot interferometer filter (green) in the light path.
5. Gently adjust the vertical position of the film, until you see interference fringes (be patient). The fringes are easily destroyed by the vibrations of the apparatus: do not lean on the microscope table, make small adjustments to the vertical position and then move your hand away from the knob and let the image settle.
6. For best results, gently adjust the tilt screws of the reference mirror until the fringes are approximately perpendicular to the film edge. You should see a fringe pattern similar to the one on the right-hand-side of Fig. 1.5.

7. Use the camera to take several snapshots of your fringe pattern. Try to time your snapshots when the building vibrations are at a minimum. You may need to adjust the contrast and exposure for best results. If vibrations prove excessive, make a short video recording, from which a few good frames may be selected later.
8. Estimate b (the fringe spacing) and a (the fringe shift) from your images. You may use any software that allows you to measure distances on screen, or print the images on paper and use a ruler to make your measurements. You should measure a distance over several fringe spacings and divide by the number of fringes to receive an average value of b . Make several measurements of the shift a and calculate the average value. The film thickness is then:

$$d = \frac{a}{b} \times \frac{\lambda}{2} \quad (1.5)$$

9. Repeat at different positions along the edge of the film. You want to be able to know both the average thickness of the film, and also have a sense of how uniform your deposition was.

References

For vacuum techniques, use books such as:

- J. Yarwood, *High Vacuum Techniques*.
- J. F. O'Hanlon, *A Users Guide to Vacuum Technology*.
- H. Mark and N. T. Olson, *Experiments in Modern Physics*, Ch. 4.

For a description of the Michelson Interferometer:

- E. Hecht and A. Zajac, *Optics*, Section 9.10.2.

Experiment 2

Resistivity and Hall effect in a thin bismuth film

Thin films are an unusual system, and often their properties are different from those of the bulk materials. In the previous experiment, a thin film sample of Bi on the glass substrate was prepared. In this experiment we will measure the basic electrical characteristic of this sample, its resistivity, using the four-point van der Pauw technique. By placing the sample in an external magnetic field of known strength we will also be able to observe the Hall effect in this thin-film sample, and to estimate such fundamental quantities as density and mobility of free charge carriers.

2.1 Introduction

The conductivity σ of a solid depends on two parameters: n , the number of charge carriers per unit volume (in metals, the free electrons are the charge carriers, of charge \bar{e} each), and the velocity with which the carriers move through the solid when an electric field is applied. The ratio of this drift velocity (in m/s) to the applied field (in V/m) is called *mobility* μ (in $\text{m}^2\text{V}^{-1}\text{s}^{-1}$). The two factors together define the *conductivity* of the material, as

$$\sigma = en\mu \quad (2.1)$$

The conductivity (or its inverse, the resistivity ρ) can in principle be determined by measuring the resistance of a block of length ℓ and cross-sectional area $A (= w \times d)$. If a current i is passed through the block, and a potential difference V is measured at two points ℓ apart along the direction of the current, then

$$\rho = \frac{V}{i} \times \frac{w \times d}{\ell}. \quad (2.2)$$

In practice one rarely has (or can make) a sample in this ideal shape, and a number of techniques are available to determine ρ from i and V measurements on samples of irregular shape. We will use a method developed by van der Pauw (1958), for isotropic ($\rho_{xx} = \rho_{yy} = \rho_{zz} = \rho$), homogeneous samples of constant thickness $d \ll \ell, w$, but otherwise of arbitrary shape.

The van der Pauw method

To do that, we will make use of four contact points, labelled A, B, C and D, on the sides of the flat sample as seen in Fig. 2.1; note that the method is restricted to the electrical contacts being at the periphery of the sample. A current i_{AB} is passed from A to B, and the resulting voltage difference V_{CD} is measured between contacts C and D; the ratio V_{CD}/i_{AB} has the dimension of “resistance”. By *reciprocity theorem* (Irwin, 1987), the same result can also be obtained as the ratio V_{AB}/i_{CD} , and the resulting resistance is, therefore

$$R_1 = R_{AB,CD} = \frac{V_{CD}}{i_{AB}} = R_{CD,AB} = \frac{V_{AB}}{i_{CD}}. \quad (2.3)$$

To compensate for voltage bias due to contact effects, one could also reverse the direction of the current and hence, the polarity of the measured voltage, thus producing a total of four possible measurements of R_1 . The best precision is obtained by taking the average of all four values.

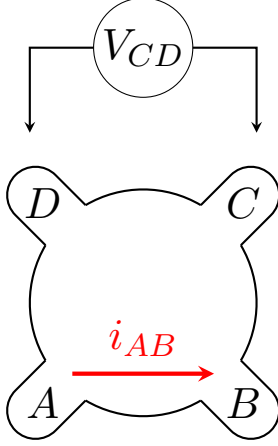


Figure 2.1: A schematic illustration of the four contact points.

Next, one can pass the current i_{BC} from B to C and measure the voltage V_{DA} or, by reciprocity, V_{BC} and i_{DA} , to determine

$$R_2 = R_{BC,DA} = \frac{V_{DA}}{i_{BC}} = R_{DA,BC} = \frac{V_{BC}}{i_{DA}}. \quad (2.4)$$

According to van der Pauw (1958), R_1 and R_2 are related to the sample resistivity ρ and thickness d by:

$$e^{-\pi d R_1 / \rho} + e^{-\pi d R_2 / \rho} = 1 \quad (2.5)$$

Equation 2.5 does not have a closed-form solution for ρ , but it can be rewritten as:

$$\rho = \frac{\pi d}{\ln 2} \cdot \frac{(R_1 + R_2)}{2} f\left(\frac{R_1}{R_2}\right) \quad (2.6)$$

where the so-called van der Pauw function $f(x)$ of the argument $x = R_1/R_2$ satisfies

$$\cosh \left[\frac{\ln 2}{f(x)} \frac{x-1}{x+1} \right] = \frac{1}{2} \exp \left[\frac{\ln 2}{f(x)} \right] \quad (2.7)$$

Values of $f(x)$ can be calculated numerically (see Julury, 2012, for matlab/octave code) or looked up in a table; for small $x = R_1/R_2$, an approximate expression $f(x) \approx 1/\cosh(\ln(x)/2.403)$ may be used, with an error of less than 0.1% for $x < 2.2$ and less than 1% for $x < 4.3$. After measuring R_1 and R_2 and calculating R_1/R_2 for the sample, its resistivity ρ can be calculated from Equation 2.6. Notice that the van der Pauw method requires the measurement of only the thickness d of the sample; the standard method involving a block of material requires three separate measurements of the sample dimensions.

The Hall effect

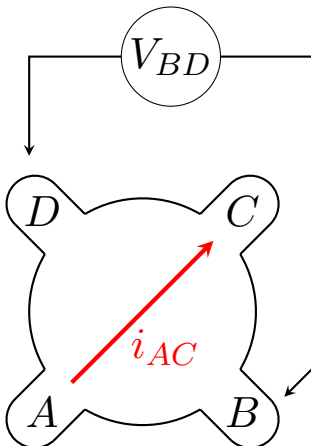


Figure 2.2: A schematic illustration of the four contact points.

The Hall effect is the sideways deflection of the moving charge carriers in the sample due to a magnetic field \vec{B} perpendicular to the current \vec{i} . An electron travelling with velocity \vec{v} in the (negative) $-x$ -direction (*i.e.*, a positive x -direction of the conventional current) experiences a Lorentz force $q\vec{v} \times \vec{B}$, with $q = \bar{e}$, in the (positive) z -direction due to a \vec{B} field in the (positive) y -direction; the result is a potential difference, the Hall voltage V_H , that develops between the sides of the sample in the z -direction. Placing the thin-film sample in an external magnetic field, with the normal to the glass slide (the y -axis) along the field, and sending a current between the two opposite contact points (i_{AC} , as in Fig. 2.2, or i_{BD}) creates a voltage ΔV_H between the other two contact points (V_{BD} and V_{AC} , respectively).

This voltage is the measure of the electrical field \vec{E} created by the sideways displacement of the electrons, and the force due to this field balances out the Lorentz force: $evB = eE$ (magnitudes only). In a “block” of material of dimensions $\ell \times A = \ell \times w \times d$, and charge carrier density n , the current i is the total charge per unit time t :

$$i = \frac{(\ell \times A)ne}{t} = vAne = v(w \times d)ne, \quad (2.8)$$

and this provides an expression for v in term of i , so the Hall voltage can be written as

$$\Delta V_H = wE = wvB = \frac{iB}{dne}. \quad (2.9)$$

The Hall coefficient R_H , defined as

$$R_H = \frac{\Delta V_H d}{iB}, \quad (2.10)$$

is directly related to the the carrier concentration n and the charge of each carrier, e , as

$$n = \frac{1}{eR_H} \quad (2.11)$$

Once n is known, the mobility μ of the charge carriers can be calculated (from Eq. 2.1) as

$$\mu = \frac{\sigma}{en} = \frac{1}{\rho en} = \frac{R_H}{\rho}. \quad (2.12)$$

2.2 Measurement checklists

Resistivity measurement

To determine ρ for a thin-film bismuth film:

1. Place the film in the sample holder and attach the four contacts A, B, C and D to the film. This is the most delicate part of the lab, as the thin layer of metal on the glass substrate is easily scratched, disrupting the continuity of the film, or even breaking the electrical contact. The best way to obtain a good contact is to:

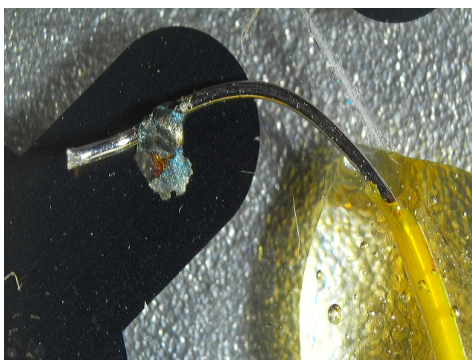


Figure 2.3: Making a good contact: note a small drop of silver paint, the epoxy holding the wire securely, and a slightly upturned tip of the wire.

- (a) use four thin (wire-wrap) wires, stripped of insulation for about one cm at the end, and slightly bent up so that the sharp tip of the wire does not scratch the sample surface;
- (b) using masking tape, tape down the glass slide by its edges; temporarily holding the wires in place with thin strips of the tape, arrange the wires to make clean contact with the four pads, and place a drop of quick-setting epoxy to fix the wires in place;
- (c) using a sharp tool (a sharpened tip of a handle of a cotton swab works well), gently place a drop of conductive silver paint onto the place where the wire touches the thin film, and let it dry; use small amounts of paint, as it shrinks a little while drying, and may crack the thin film disrupting the electrical continuity;

- (d) use an ohmmeter to verify that all four wires make electrical contact with the sample; if needed, repeat the previous step, spreading the silver paint until the contact is good; be careful not to short nearby wires.

An alternative method is to solder the wires into place using indium as solder. The process is delicate and requires precise temperature control of the tip of the soldering iron, so that it is just hot enough to melt In, but not so hot as to melt the Bi film underneath it. If you have some experience in soldering, this may prove to be a superior technique, but complete novices usually find the silver-paint method simpler. Note that in both cases it is necessary to provide good strain relief by placing a drop of epoxy to hold wires in place on the glass slide.

2. Measure i_{AB} and V_{CD} using a current source, an ammmeter in series, and a voltmeter, and calculate R_1 . Reverse the direction of the current leads and determine R_1 again. The two values of R_1 should be identical unless you have poor point contacts that act as tiny diodes. The best results are obtained by systematically varying the current and fitting a straight line to the resulting data set that includes all of the data, for both current directions. Repeat for i_{CD} and V_{AB} .
3. Similarly determine $R_2 = I_{BC}/V_{AD}$; also check for $R_2 = i_{AD}/V_{BC}$. Calculate average values of R_1 , R_2 and R_1/R_2 .
4. Determine the appropriate value for the van der Pauw function $f(R_1/R_2)^1$ for your sample and calculate ρ .

Hall-effect measurement

To determine n and μ for a thin-film bismuth film:

1. To observe the Hall effect, apply a current i_{AC} and measure the voltage V_{BD} . Place the sample between the poles of the electromagnet (you can use masking tape to tape the sample to the center of the pole of the magnet), which puts the magnetic field \vec{B} along the normal to the sample. Measure i_{AC} and V_{BD} for several values of \vec{B} ; the measured voltage changes to a new value $V_{BD} + \Delta V_H$.
This can be repeated for a range of currents i_{AC} . Reverse the direction of the current to check for non-Ohmic (diode-like rectifying) contacts. Swapping the electromagnet leads at the power supply (but making sure to turn the magnet current down to zero first!) allows for reversing the direction of the magnetic field, and of the sign of ΔV_H to compensate for thermoelectric effects at contact points or other sources of voltage bias.
2. Similar values can be obtained by applying the current i_{BD} and measuring the resulting voltage V_{AC} . Reconnect the leads to measure i_{BD} , and V_{AC} , and measure ΔV_H again. Again, reverse the direction of the current i_{BD} , and/or reverse the direction of the \vec{B} -field as well as vary its strength to change the sign of ΔV_H .
3. The Hall coefficient R_H is related to ΔV_H by:

$$\Delta V_H = R_H \frac{i_{AC} B}{d} . \quad (2.13)$$

Calculate R_H using the average of ΔV_H values obtained in the previous two steps, or by performing a fit to $\Delta V_H = \Delta V_H(i_{AC}, B)$ using R_H as a parameter of the fit, and calculate n and μ for Bi, using Eqs. 2.11–2.12. Compare n (the number of “free” electrons per unit volume) to the number of Bi atoms per unit volume.

Be sure to include the tables with raw V and i values in an Appendix of your lab report.

¹Pre-calculated values can be downloaded from https://juluribk.com/images/van_der_pauw_correction_factor.csv and plotted or interpolated numerically.

References

1. D. Halliday and R. Resnick, *Fundamentals of Physics*, Chapters 28, 30-4.
2. K. Seeger, *Semiconductor Physics*, Chapter 4.3.
3. E. H. Putley, *The Hall Effect and Semi-conductor Physics*, Chapters 1-2 and 2-1.
4. Van der Pauw, L.J. A method of measuring specific resistivity and Hall effect of discs of arbitrary shape. *Philips Research Reports*, **13**:1-9, 1958.
URL: <http://electron.mit.edu/~gsteele/vanderpauw/vanderpauw.pdf>
5. B. Julury. van der Pauw correction factor. 2012.
URL: <https://juluribk.com/van-der-pauw-correction-factor.html>
6. J. D. Irwin, *Basic Engineering Circuit Analysis*, 2nd ed. Macmillan, New York, 1987. Chapter 15.

Experiment 3

Gamma-ray scintillation spectroscopy and the Compton effect

This experiment uses several sources of ionizing radiation. You must have completed your radiation safety training before you start.

The experiment is in two parts: first we calibrate the spectrometer by measuring the spectra of several sources of known γ energy, and then use it to precisely measure the way photons scatter off of an Al target, as a function of the scattering angle, and thus to identify the Compton scattering mechanism.

3.1 The scintillation spectrometer

The spectrometer is designed to record and display the spectrum of γ -rays emitted by radioactive sources. The energies it can detect cover the range from about 10 KeV (X-rays) to nearly 10 MeV. The use of energy units, rather than the wavelength or frequency of the EM waves, for the classification of the emissions from radioactive materials, emphasises the particle-like interaction of γ -rays with matter.

There is no dispersive element, such as a grating or a prism, in the spectrometer; there are no slits, lenses or mirrors. The detector is a crystal of thallium-doped sodium iodide, NaI(Th). When radiation, in the form of an X-ray or γ -ray photon, or an energetic electron, interacts with the crystal a certain fraction of the energy deposited in the crystal is transferred to the thallium activation centres and subsequently emitted as visible light. Other fractions of the deposited energy are dissipated as heat or through re-radiation in the invisible portions of the spectrum. The total energy deposit is itself proportional to the incident photon energy. The number of visible light photons emitted by the activation centres is directly proportional to the amount of energy deposited and, hence, to the energy of the incident radiation.

Each group of photons emitted by the centres appears as a short flash of light, or scintillation. The photons are detected by a photomultiplier tube (PMT) which produces a voltage pulse with height proportional to the number of photons that entered the tube. Hence, the height of the voltage pulse is proportional to the energy deposited in the crystal. If the dimensions of the crystal are such that the incident radiation is completely absorbed (*i.e.*, the probability of absorption approaches 1), the height is proportional to the energy of the incident radiation. The number of voltage pulses per second with heights lying between V and $V + dV$ (this defines a single “channel” of voltage and, therefore, of energy) is counted electronically. This measures the intensity (number of photons) as a function of energy, *i.e.* the energy spectrum of the radiation. The device that performs the counting and recording function is called a multi-channel analyzer (MCA). The MCA, the detector crystal, and the photomultiplier form the γ -ray spectrometer.

If a source of monoenergetic γ -rays, such as Cs^{137} , is examined with the spectrometer it is found that the recorded spectrum contains a fairly well-defined peak at some channel number, and a broad continuum of smaller peaks that extends from the main peak toward lower channel numbers (lower energies). The origin of these features of the spectrum is found in the nature of the interactions of γ -rays with the crystal, which can occur in one of the following three ways:

1. Photoelectric Absorption. The γ -ray is annihilated and the energy of the photon is transferred to an electron bound to an atom or ion of the crystal. The kinetic energy of the electron (KeV to MeV), plus its binding energy to the atom or ion (eV), is equal to the energy of the γ -ray photon. This

photoelectron then transfers, on average, a certain fraction of its energy to the thallium activation centres as it moves through the crystal. In crystals of the sizes used in practice the photoelectron loses all its kinetic energy within the crystal. The number of photons emitted by the thallium centres is proportional to the γ -ray energy. The voltage pulse at the output of the PMT that collects the light from the NaI(Th) crystal is proportional to the γ -ray energy.

2. Compton Scattering. The γ -ray transfers momentum to an electron and is thereby “scattered” with lower energy and momentum. The scattered electron will excite some thallium centres and cause a voltage pulse to appear at the PMT output. The scattered gamma photon may then interact by photoelectric absorption (see 1.) and produce a PMT voltage pulse. The height of this pulse, as well as that produced by the interaction of the scattered electron with the crystal, will be less than that produced when the gamma photon energy is deposited as in the previous case. Since the loss of energy by the gamma photon depends on the scattering angle, there will be a range of pulse heights detected.
3. Pair Production. When a photon of energy greater than or equal to twice the rest energy of an electron interacts with matter it may be annihilated. The photon energy appears as a positron electron pair. When the positron meets another electron a gamma photon (annihilation radiation) appears. For our purposes this effect may be ignored because the gamma sources used do not have a sufficient energy.

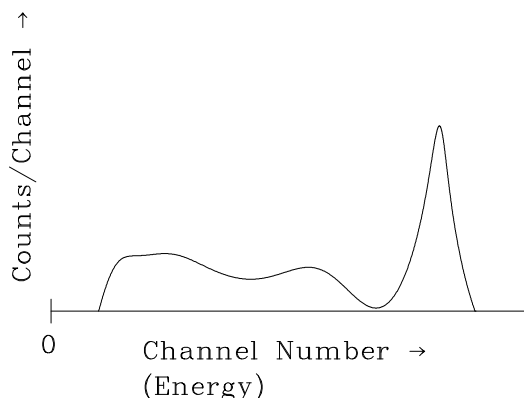


Figure 3.1: A sketch of a ^{137}Cs spectrum

A typical spectrum for a cesium ^{137}Cs source is shown schematically in Fig. 3.1. The large peak at high energies (channel numbers, pulse heights) arises from mechanism 1. It is called the Full Energy Peak. The energy corresponding to the maximum intensity is the energy of the gamma photon. The “shoulder” of the peak on the lower-energy side is the so-called Compton Edge. It is produced by the most energetic electrons arising from the Compton scattering process. The secondary peak at still lower energy arises from the full energy peak of the back-scattered photons in the Compton process. Other lower energy peaks may arise from X-rays produced in the PMT shielding or from background effects, and they can be quite strong. However,

the spectrometer can be set to ignore the peaks of energy below a certain limit, to focus on the high-energy γ -ray peaks: note the region of zero intensity near the zero of the energy axis in Fig. 3.1. Identifying the channel number of the full-energy peak and knowing its true energy from reference sources provides a way to calibrate the spectrometer.

Spectrometer calibration checklist

The scintillation crystal and PMT are housed in a protective lead shield. The signal output from the PMT is a pulse where the peak voltage is proportional to the photon energy absorbed by the crystal.

The XIA Saturn hardware incorporates the MCA electronics as well as a programmable-gain PMT amplifier and a PMT voltage source, in a single compact box, so all controls are in one place. The anode voltage of the PMT has been set to the optimum value of 1,000 V and is not adjustable. The gain of the pre-amplifier that connects the PMT to the spectrometer (ORTEC model 113) sets the range of voltages



Figure 3.2: Main and Plot menu windows of EPICS

(pulse heights) for the energy spectrum. If the gain setting is altered, the spectrometer will require a re-calibration.

The software that controls the spectrometer (EPICS) is the same software used at large nuclear physics laboratories, and is capable of controlling dozens of sensors and mechanical and electronic actuators simultaneously. In our lab, only a small subset of the available parameters will be used, and each of the data acquisitions (“scans”) will contain only a single spectrum. XIA Saturn MCA has 2048 energy channels, sufficient for the energy resolution of our detector.

- Turn on the XIA Saturn, then press the red button. The PMT voltage will slowly ramp from 0 to 1,000 V. At the end of the experiments you will press this button to turn the high voltage off; please wait until the voltage actually ramps down before turning off the power switch.
- Collect a set of calibration sources from the instructor; they are kept in the vault and must be returned at the end of the experiment. The following steps must be performed for each of the sources in turn.
- Place a calibration source near the crystal end of the detector. The active end is the blackened end of a plastic rod. You can simply lay it down in the lead shielding surrounding the PMT.
- Invoke the software; and icon called “XIA Saturn” should be on the desktop. The main control window appears, as shown on the left in Fig. 3.2. During the experiment you will make use of additional sub-menus that will open up as separate windows; the two most important ones are the **Scans** and **Plots** sub-menus. Click on **Plots** to open the MCA display window shown on the right in Fig. 3.2 and on **Scans** to open the scan control window shown on the left in Fig. 3.3. The spectrometer console has an extended display, you will find it helpful when multiple windows are open. While you wait during data acquisitions, you may want to perform other tasks, such as preliminary data analysis on already acquired partial data.
- You should not need to make any adjustments to the default settings with the exception of the following:
 1. the **Elapsed Mode** sets the duration of the data acquisition to end after a set time or to continue until the user manually stops the process. Set the mode to perform a Real Time acquisition of

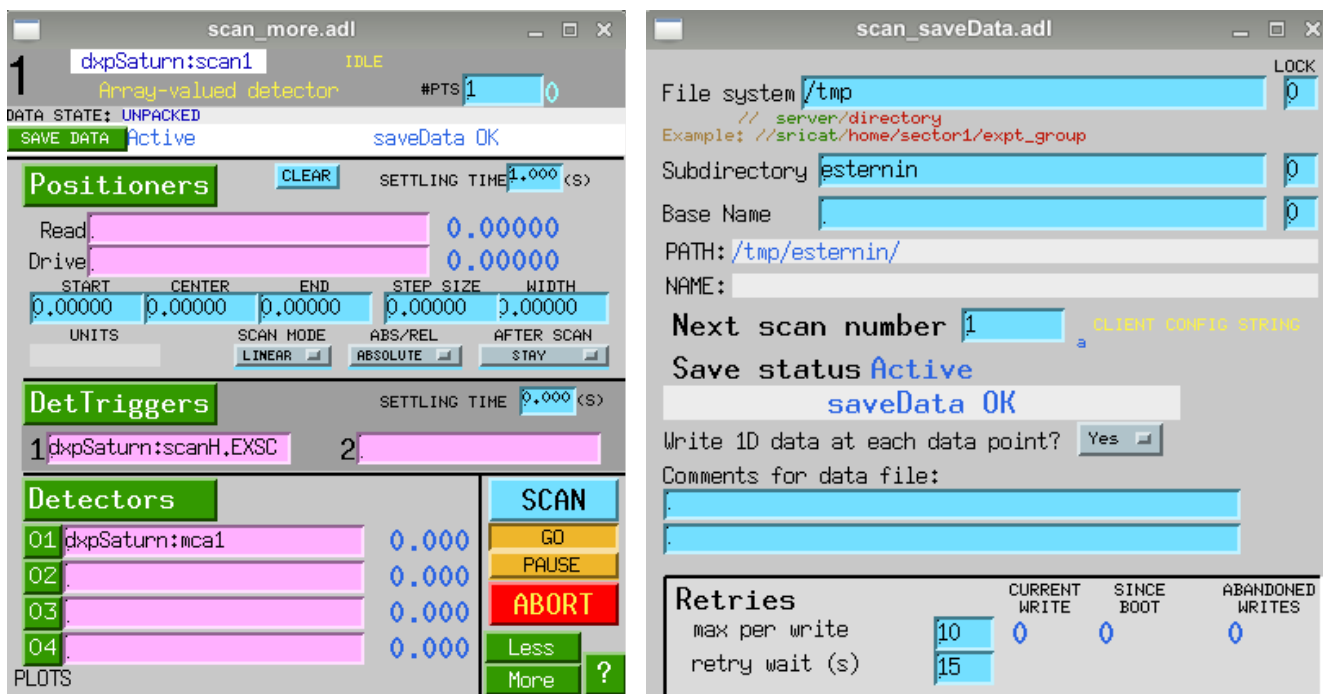


Figure 3.3: Scan and file save windows

20 seconds;

2. the **Max. energy (keV)** adjusts the energy/channel scaling of the 2048-point MCA and must be set to cover the range that includes the full energy peak of the most energetic of your calibration sources. Once set, it should not be changed, or a re-calibration will be required;
 3. the **Energy Threshold** can be adjusted to ignore low energy channels near zero where significant background noise can be present.
- Within the scan control window click on **SAVE DATA** to open the settings window for data file management, shown on the right in Fig. 3.3. You should change the default save directory to a new folder; something like `/work/3P91/2020-2021/G1/` is a good choice, as it will allow you to access your data from any workstation in the Physics cluster. Make sure that the directory you are specifying here actually exists, create it if necessary.
 - Press **Start** to accumulate a trial spectrum. This can be achieved from any of several windows, as the buttons are duplicated for convenience.
 - When you have a good estimate of the time it would take to get a clean-looking spectrum, with a clearly identified peak that can be used for calibration, adjust the acquisition time and press **SCAN** to record and save the spectrum. Depending on the strength of the signal (calibration sources become weaker with age, as they radioactively decay) you may need anywhere from 30s to 300s. Note the isotope and its γ -energy, the file name (the file names contain an index number that is incremented after each run, automatically) and the approximate channel number for the full energy peak.
- Repeat these steps for all the sources in the calibration set.

- Use fitting and plotting software (such as **physica** or **extrema**) to fit a Gaussian lineshape to each full-energy peak, and obtain an error estimate. You may start by using the prototype scripts in `/work/3P91/Compton/Demo/`; copy them into your filespace and copy the data you have acquired into the same location, using `mda2ascii` command. You may work on your data analysis while waiting for the next data scan to complete, by using `ssh -Y ab00cd@localhost` command without

Isotope	γ -energy, MeV
^{109}Cd	0.088
^{57}Co	0.1222
^{133}Ba	0.356
^{22}Na	0.5110034
^{137}Cs	0.66164
^{54}Mn	0.834827
^{60}Co	1.1732, 1.3325

Table 3.1: A selection of well-known gamma energies.

leaving the spectrometer console, or you may log onto a second workstation to access the data being saved into `/work/3P91/2020-2021/G1/` directory.

The data files saved by EPICS (`.mda`) are binary files, for reasons of compactness. To extract a readable set of numbers, suitable for plotting and analysis, a small utility, `mda2ascii`, is available on every workstation in the Physics cluster. Here's a self-explanatory sequence of steps, to perform from a terminal window, using the above example names:

```
$ ssh -Y ab00cd@localhost
Password:
$ mkdir -p 3P91/Compton
$ cd 3P91/Compton
$ mda2ascii -i 1 -o Ba-131 /work/3P91/2020-2021/G1/dxpSaturn_0001.mda
```

This places a readable data file `Ba-131.1.asc` into your directory `/home/ab00cd/3P91/Compton/`. You can now read this data file into `physica`, or `extrema`, or `gnuplot`, or another plotting/analysis software. If you are using `physica`, the two files `/work/3P91/Compton/Demo/*.pcm` will prove a handy starting point, and can be copied into the same directory. `gamma.pcm` is the top-level script; it in turn calls a subroutine in `gfit.pcm`. You can also make use of this subroutine in your own scripts.

- Plot a graph of known gamma energy *vs.* the full-energy peak channel number and fit a straight line through the data; this is your calibration curve that can be used to correctly display and analyze the spectra from the next part of the experiment.

Some of the known gamma energies you may need are listed in Table 3.1. Additional values may be obtained from sources listed in References.

? Discuss in your lab report: why is the full energy peak not sharp?

3.2 The Compton effect

The Compton effect can be studied and the scattering relationship verified. The apparatus has been set up as shown in Fig. 3.4. You will measure the energy, E' , of the scattered gamma photons as a function of their scattering angle θ . The experimental arrangement is shown in Fig. 3.4.

Note: The 25-millicurie source (inside a yellow-coloured lead brick) produces an intense collimated beam. **DO NOT** stand in the direct line of the beam **E**. **DO NOT** tilt or drop the yellow lead brick, as the high-intensity source may fall out of it. If this happens, leave the area immediately and inform the instructor.

Both **S** and **D** are well shielded with lead. The source shielding minimizes the radiation intensity in all directions except within a small solid angle centred on the beam direction, **E**. The detector shielding

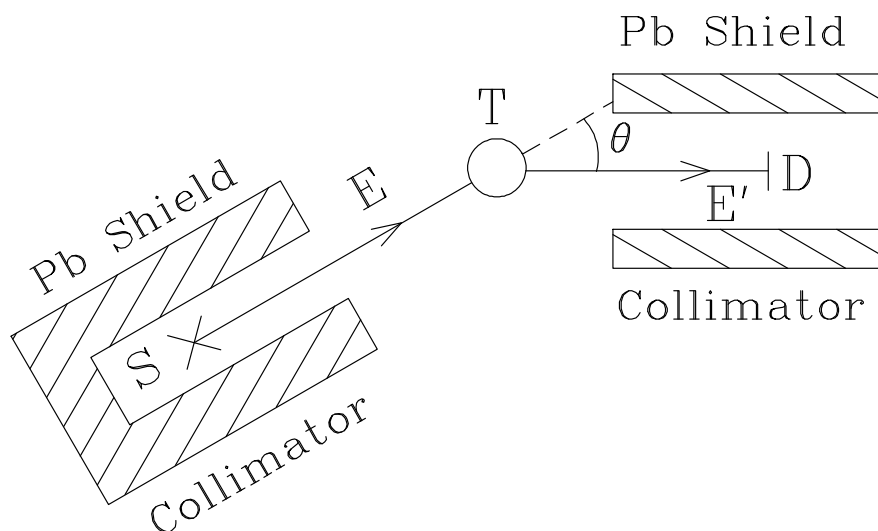


Figure 3.4: The Compton scattering apparatus. Here **S** is a ^{137}Cs γ -source, energy 0.66164 MeV, strength 25 millicuries; **E** is the collimated γ -photon beam of energy E ; **T** is the Al target that contains the free electrons from which the γ -rays scatter; **E'** is the scattered beam of photons of energy E' ; **D** is NaI γ -ray detector.

is designed to admit the scattered photons, **E'**, and to exclude entrance to photons incident from other directions. The scattering angle, θ , is varied by rotating the source assembly, **S**, about the target position, **T**. To measure **E'** use the energy calibration that you completed in the first part of the experiment.

The Compton experiment checklist

- Accumulate a series of spectra of the scattered photons as a function of the scattering angle and so determine $E'(\theta)$. The Compton formula is usually given in terms of incident wavelength λ and scattered wavelength λ' :

$$\lambda' - \lambda = \frac{h}{m_0 c} (1 - \cos \theta). \quad (3.1)$$

Show that in terms of photon energies E' and E this formula becomes

$$\frac{1}{E'} - \frac{1}{E} = \frac{1}{m_0 c^2} (1 - \cos \theta) \quad (3.2)$$

- Plot your experimental data as $1/E'$ versus $(1 - \cos \theta)$ and from the results determine E and the electron rest mass energy $m_0 c^2$.

The minimum value of the scattering angle θ at which the Compton scattering energy shift is observable will be determined by the energy resolution of the detector and the effectiveness of the lead collimator which defines the solid angle of emergence of the cesium photon beam. If the scattering angle is made too small, the direct beam of the cesium gamma photons into the detector will completely mask the small Compton energy shift. In practice it means that scattering angles below 10° are not detectable in our apparatus.

Remember that only a small fraction of the photons are scattered in the target. The intensity of the scattered beam is much less than that of the incident beam, and thus the recording time required to obtain a satisfactory spectrum may be many minutes. A direct beam into the detector would produce an intense spectrum in seconds rather than minutes!

References

- A discussion of the scintillation detector is given in: *Radiotracer Methodology in Biological, Environmental and Physical Sciences*, C. H. Wang, D. L. Willis and W. D. Loveland (Prentice-Hall), Chapters 4, 6, 7, 12. Call Number QC 795.42 W36 1975.
- A useful online source of select gamma energies is <https://www.cpp.edu/~pbsiegel/bio431/genenergies.html>.
- A comprehensive searchable database of nuclear data is maintained at Lund University, Sweden, <http://nucleardata.nuclear.lu.se/toi/>.
- EPICS software has a home here: <https://epics-controls.org/>, and the technical documentation for the XIA Saturn driver for EPICS, by Mark Rivers at U. Chicago is here: <https://www.physics.brocku.ca/Courses/3P91/References/MCA/>.

Experiment 4

Energy-dispersive X-ray diffraction

X-ray fluorescence (XRF) and X-ray diffraction (XRD) may be used to determine the constituent elements and the crystalline structure of materials.

4.1 Introduction

X-ray fluorescence

XRF refers to the absorption of incident X-rays ($h\nu_0$) resulting in the production of a set of X-rays whose energies ($h\nu_j$) are characteristic of the absorber atom(s) (Z). The characteristic X-rays can therefore be used to identify the atom(s) present in the sample.

The incident X-ray photon ($h\nu_0$) undergoes a photoelectric interaction with a target atom (Z) resulting in the annihilation of the photon and ionization of the target atom. The energy equation is

$$K = h\nu_0 - B$$

where K is the kinetic energy of the photoelectron liberated from the atom and B is its binding energy to the atom. Subsequently, the ionized atom combines with an electron and undergoes a de-excitation to its electrically neutral ground state. X-ray photons, whose energies ($h\nu_j$) are characteristic of the target atom (Z), are produced in the de-excitation. An energy level diagram is shown in Fig. 4.1. Each level

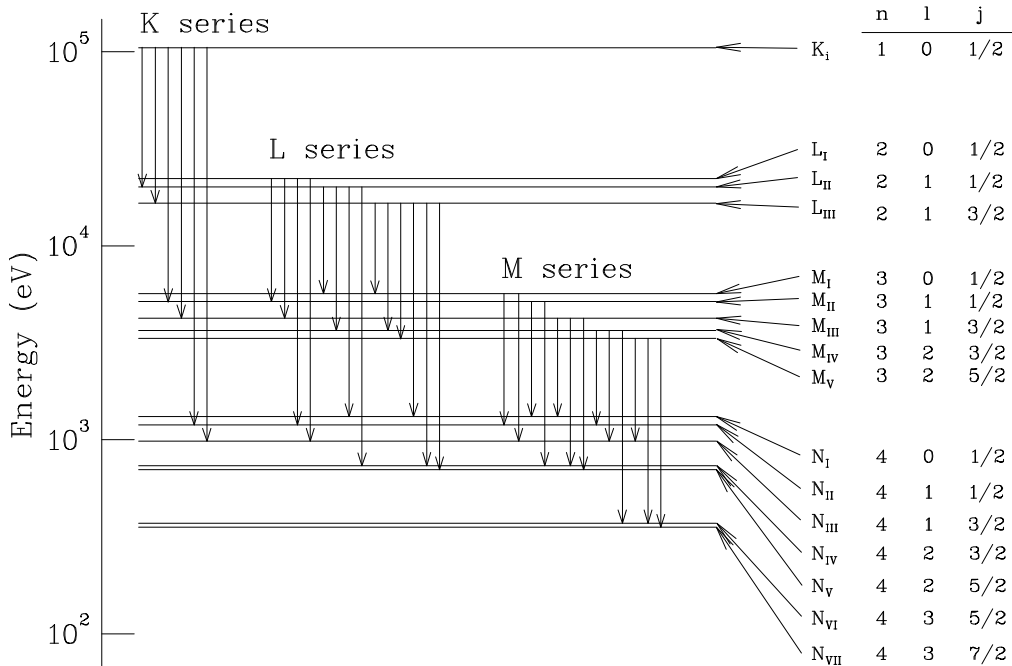


Figure 4.1: A schematic diagram of the X-ray energy levels

corresponds to the excitation of the atom when a single electron is missing from the otherwise full subshell (nlj). Zero energy corresponds to the ground state of the neutral atom. Level K , corresponds to the

binding energy (B_K) of an electron in the K shell. There are three closely spaced L -shell levels labelled L_I, L_{II}, L_{III} corresponding to slightly different L -shell electron binding energies. If

$$h\nu_0 > B_K$$

then all characteristic X-rays (K -series, L -series, *etc.*) are produced. If

$$B_L < h\nu_0 < B_K,$$

then the K -series X-rays are not produced.

X-ray diffraction

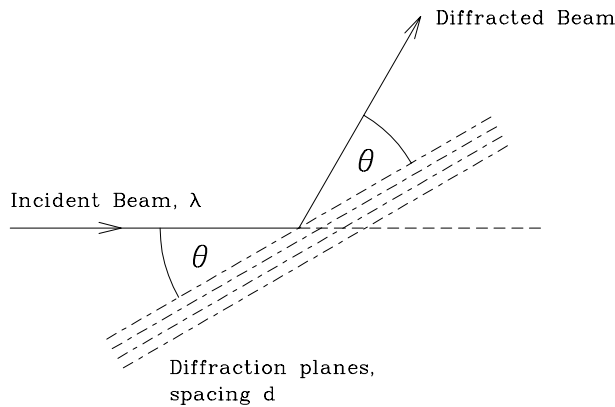


Figure 4.2: Geometry of X-ray diffraction

X-ray diffraction is used extensively to determine the structure of crystalline and also of non-crystalline and amorphous materials. For crystalline materials, the direction θ and wavelength λ of the diffracted beam are related by Bragg's Law; with reference to Fig. 4.2, this is

$$2d \sin \theta = n\lambda$$

where n is the order of diffraction from crystalline lattice planes of spacing d . The equation may be rewritten as

$$2d_n \sin \theta = \lambda \quad (4.1)$$

where $d_n = d/n$ and the equation now represents first order diffraction from planes d/n . Using

Bragg's Law, a measurement of θ and λ for a diffracted beam enables the spacing d_n to be determined. For cubic lattices,

$$d = \frac{a}{\sqrt{h^2 + k^2 + l^2}} \quad (4.2)$$

where a is the side length of the cubic lattice cell (the lattice constant), and h, k and l are the Miller indices of the lattice planes.

4.2 The apparatus

An overview of the apparatus is shown in Fig. 4.3. The incident beam produced by the X-ray machine has its intensity continuously distributed over a range of X-ray photon energy up to a maximum value eV , where V is the voltage of the X-ray tube. This voltage accelerates a beam of electrons that is directed vertically upward to strike a Cu target; the impact generates X-rays that exit the head atop the X-ray machine horizontally through a thin collimator tube as a narrow focused beam. The front panel controls enable the user to set the value of the voltage that determines the energy of the X-ray photons, the operating current that determines the intensity of the beam (number of photons per second), and two independent controls that need to be set to open for the X-ray beam to emerge: setting the port to open allows the beam of electrons to hit the Cu target and to generate the X-rays, and setting the shutter to open allows the generated X-ray to emerge through the collimator. The initial turnkey switch automatically starts the cooling water flow through the X-ray tube; this should be visually verified before operating the X-ray machine, and one should wait for the water to run cold before turning the switch to off.

The incident beam strikes a crystalline powder sample that is mounted using a dual-sided tape to a sample holder atop a large cylindrical enclosure, seen in Fig 4.4. The enclosure contains two narrow

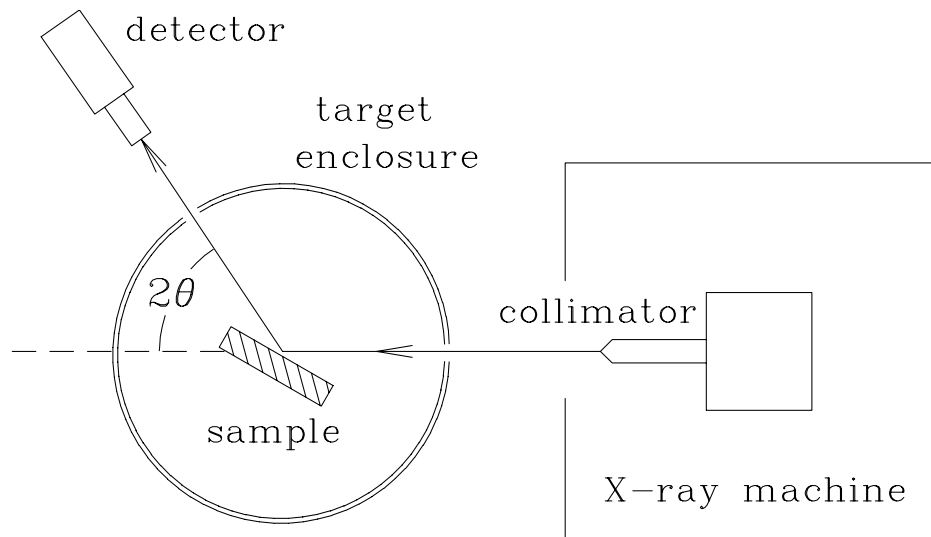
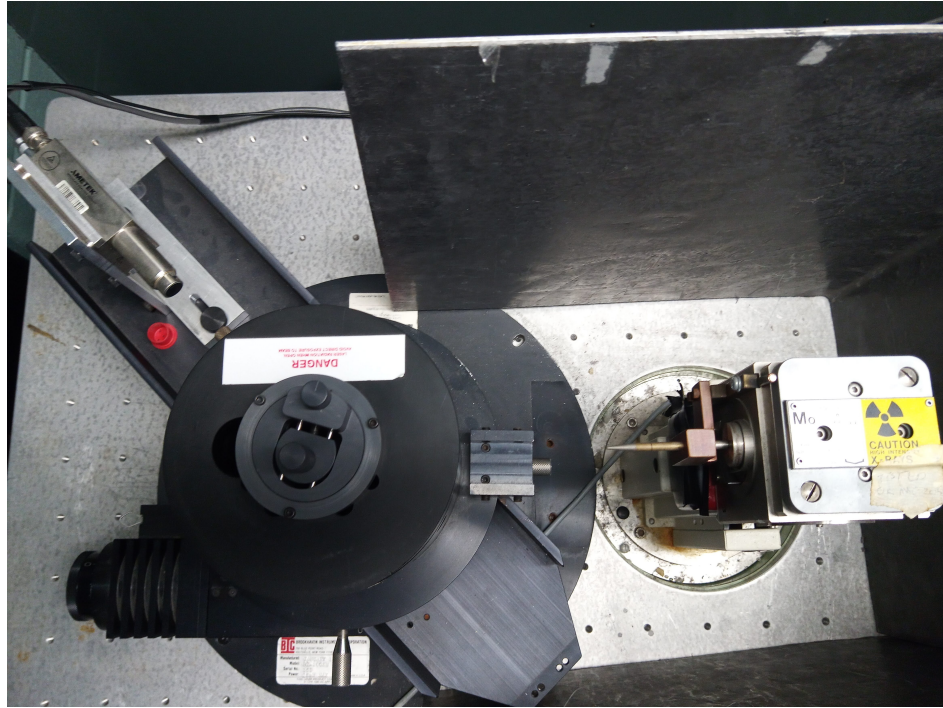


Figure 4.3: A top view (lid removed) and a schematic diagram of the X-ray apparatus.

openings for the incident and the scattered beams as well as two positioning control knobs that allow changes to the orientation and the forward displacement of the sample holder. These controls allow the user to optimize for maximum intensity at the detector; usually this is done on a known sample with a strong signal. As the samples are replaced it is desirable to place the front surface of the sample into the exact same position, so different samples may be placed on spacers, to keep the overall thickness approximately constant.

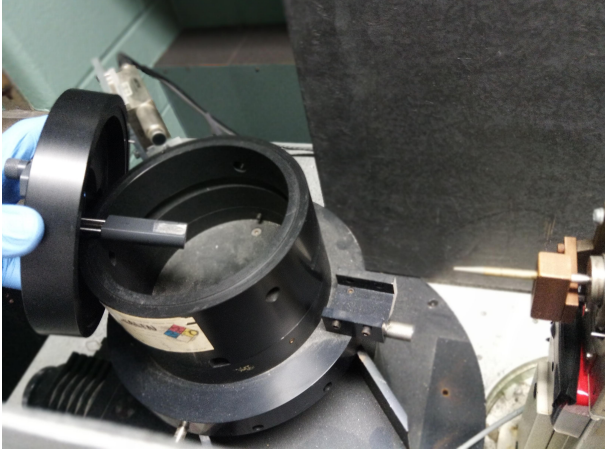


Figure 4.4: The target enclosure with its lid lifted. The sample holder is suspended from the lid of the enclosure. Two knobs on top control the vertical position and the forward displacement of the target attached to the lower end of the sample holder.

Fig. 4.5 is identical to that experiment and will not be described here. Note also that the scripts developed to analyze the data from that experiment will be usable for this experiment with only minor modifications.

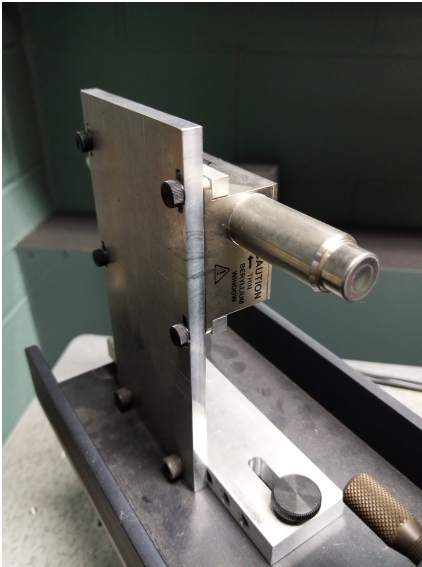


Figure 4.6: The solid-state detector.

The spectrum $I(E)$, *i.e.* the number of photons detected as a function of photon energy, consists of a series of relatively narrow peaks superimposed on a smoothly varying background. The peaks arise from

- X-rays fluoresced from the target atoms,
- X-rays diffracted from the crystal lattice.

The position of the peak on the MCA energy scale is a measure of the corresponding photon energy.

Energy Dispersive X-ray Diffraction

In this apparatus, the diffraction is observed by measuring $I(E)$ while keeping θ constant. Bragg's Law may be rewritten in terms of the diffracted beam photon energy, E , as

$$2d_n \sin \theta = \lambda = \frac{hc}{E} \quad (4.3)$$

or

$$E_{hkl} = \frac{hc}{2 \sin \theta} \times \frac{1}{d_{hkl}}. \quad (4.4)$$

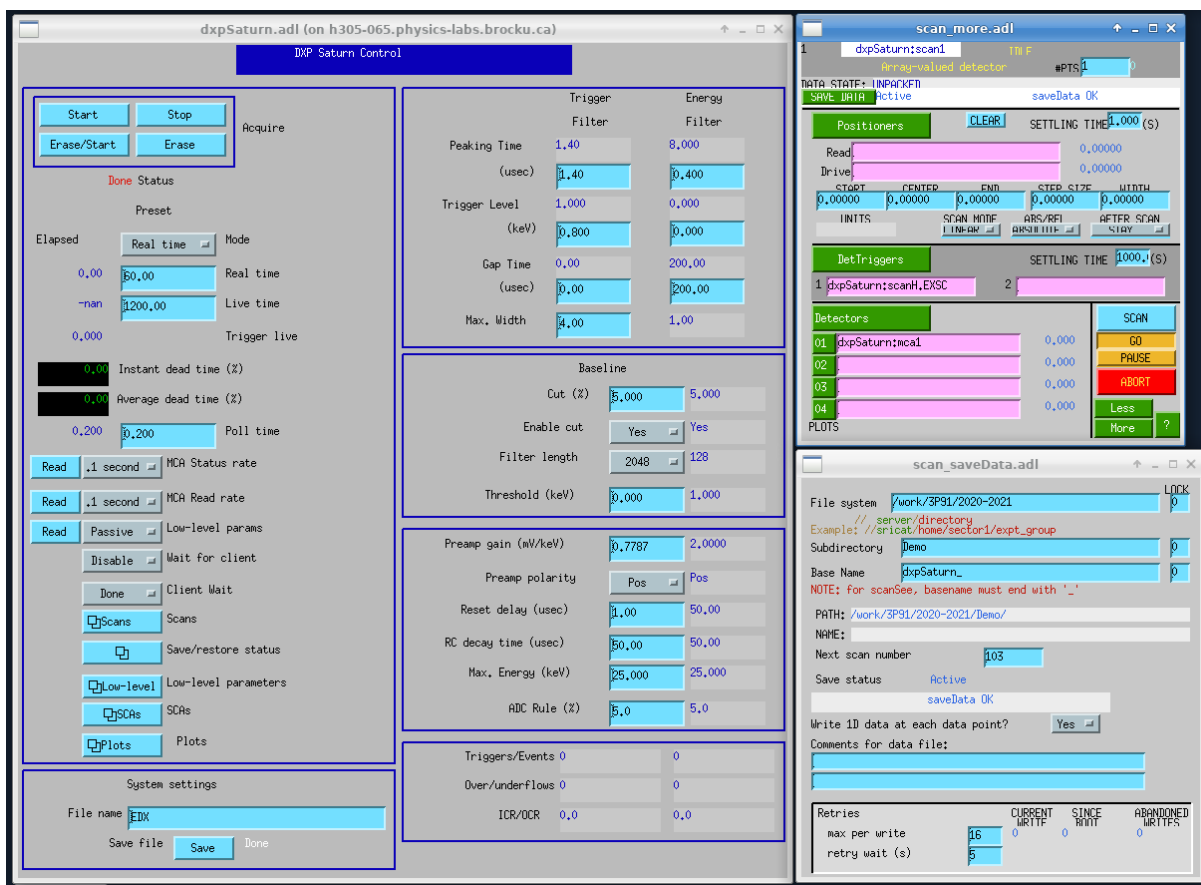


Figure 4.5: The EPICS software interface. MCA display is found under the button "Plots".

Here hkl are the Miller indices of the planes which produce diffraction of photons of energy E_{hkl} . For a particular value of the diffraction angle θ (the detector is positioned at a fixed angle 2θ relative to the incident beam) diffraction from planes with different d_{hkl} values produce diffraction peaks at energies E_{hkl} , given by Eq. 2.1. Diffraction peak energies E_{hkl} are a function of θ (Eq. 2.1); XRF characteristic peak energies are independent of θ . In addition, the diffraction peak intensities are normally much weaker than those produced by the characteristic X-rays fluoresced from the target. Either of the above features may be used to differentiate characteristic X-ray fluorescence and diffraction features in the spectrum.

4.3 Measurement checklist

CAUTION

The instructor will demonstrate the operation of the X-ray machine, the solid-state photon detector and the multichannel analyser. Under no circumstances is the apparatus to be operated prior to instruction. Under no circumstances are adjustments to be made to the target arrangement with the X-ray beam on. The X-ray beam is a radiation hazard. Lead-lined enclosure should always be in place whenever the X-ray beam is on. Radiation exposure badges must be worn by the operator. Failure to maintain radiation safety protocols will result in an immediate involuntary withdrawal from the course.

The objective is to identify the constituent elements (using XRF) of unknown powdered samples. To do that, a series of samples with known XRF energies must be used to first calibrate the MCA energy scale.

Operating the X-ray machine



Figure 4.7: The front-panel controls of the X-Ray machine.

1. Verify that the HV control is set at zero and use the turnkey to turn the machine on. Verify that the cooling water is flowing freely into the drain.
2. Slowly turn up the voltage and current settings to the operational values. The machine is normally operated at a tube voltage of 20–30 kV and a current of up to a maximum of about 15 mA. These values are not at all critical; this voltage range provides an incident X-ray beam spectrum which is reasonably well-matched to that required for both XRF and XRD, and the current setting produces the intensity of the beam that keeps the spectrum acquisition times reasonably short, 30–300 s.

- Align the target. Note that it may be well-aligned by the previous experimenter, so you may want to skip this step initially, and check the strength of the signal from a well-known sample first, but be sure to be able to perform this step if necessary.

Note: The X-ray beam port and shutter must both be *CLOSED* and the X-ray tube high voltage turned OFF prior to making any beam/target alignment changes. This is **mandatory**.

Alignment (*X-ray HV OFF; beam port and shutter CLOSED*): position, visually, a calibration target into the X-ray beam path (which is determined by the axis of the X-ray beam collimator) and set the solid-state detector rotatable platform somewhere in the range $2\theta = 45^\circ\text{--}60^\circ$ relative to the incident X-ray beam path. Check visually, but carefully, that the X-ray beam path strikes the target surface centrally and also that the target surface can be seen by the Si detector. A laser pointer may be useful here. It is not necessary to set a precise value of 2θ ; knowing the approximate value (\pm a few degrees) may be helpful in identifying features of the diffraction spectrum.

Energy Calibration

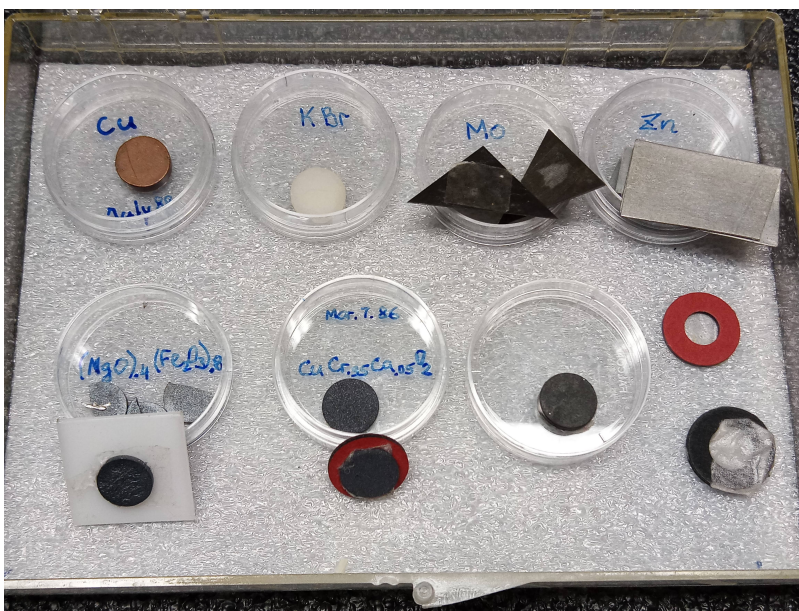


Figure 4.8: A typical sample kit. Note the mounting supports under some of the samples, and extras at lower right.

For the calibration, use samples of Zn, Mo and KBr, others as available. Fig. 4.8 shows a typical sample set made available for this experiment. Be sure to not mix up the samples when replacing them in their respective containers. Some of the samples are of very high purity or may be fragile, be sure to wear gloves and handle the samples with care. For fragile samples, always pre-mount them using mounting supports (washers, teflon sheet pieces), do not mount or peel off the samples directly from the sample holder.

- Spectrum acquisition (*X-ray HV ON; beam port and shutter OPEN*): acquire a “smooth”-looking spectrum in which the peaks are clearly defined, that is the peak locations can be determined by inspection to ± 1 channel number. The XRF lines due to the main elements in the layer are normally significantly stronger than any diffraction lines.

When the accumulation is completed, set the beam port and shutter to *OFF*. In addition, set *HV OFF* before changing the sample.

- Record the channel number n for each of the XRF peaks and identify the peaks with the characteristic energies E_n corresponding to the known elements in the calibration target. You may use plotting

and fitting software to refine your values. A copy of the “X-ray Data Booklet” is made available, use it to supply the true energies of the identified peaks, and establish a calibration relation

$$E_n = a \times n + b$$

with the calibration constants a and b . This calibration can be used throughout the experiment, providing the gain of the detector amplifier and the configuration settings of the MCA remain unchanged. Using the calibration, the energies of XRF and diffraction peaks obtained subsequently in the spectra of other materials may be determined.

6. Diffraction peaks: using the value of d that corresponds to the highest intensity in the calibration samples and an estimated value of 2θ , calculate E_{hkl} values from Eq. 4.4, thus establishing the energy where a diffraction peak might be located. Inspect the $I(E)$ spectrum for such (weak) peaks. If one (or more) are found, change 2θ (by a few degrees) and re-acquire the spectrum to verify that, indeed, the peak energy shifts, *i.e.* is a function of θ .

Analysis of powder samples

7. Alignment (*X-ray HV OFF; X-ray beam port and shutter CLOSED*): install the powdered crystalline target and repeat the beam-target-detector alignment described in step 3.
8. Spectrum acquisition (*X-ray HV ON, X-ray beam port and shutter OPEN*): acquire a spectrum; strong XRF lines and (possibly) much weaker diffraction lines should be visible. Change the detector angle by a few degrees and repeat the accumulation; compare with the previous spectrum. The diffraction peaks shift position in the spectrum, the XRF peaks do not. After this provisional classification into XRF and diffraction lines, keep the detector angle fixed and accumulate until a “smooth” spectrum is obtained. A “smooth” spectrum is a very qualitative term which simply means that the centres of the peaks of interest may be determined by visual inspection to approximately ± 1 channel.
9. Shutdown: when the data acquisition has been completed, close the X-ray beam port and shutter, turn the X-ray current and HV OFF, dial voltage and current controls down to zero, wait for the cooling water to run cold, and turn off the X-ray machine.

Data Analysis

10. Determine the energies of the XRF and diffraction peaks (if any).
11. Using the characteristic X-ray energy tables (see the *X-Ray Data Booklet*), identify the elements in the powder samples. Several samples are provided, some with an expected composition specified and one “unknown”. Verify the presence of the elements in samples of known composition, and determine the composition of the unknown sample.

References

- *X-Ray Data Booklet*, Center for X-Ray Optics and Advanced Light Source, Lawrence Berkeley National Laboratory, University of California, Berkeley, CA. 2009. A copy is available at the console of the X-ray spectrometer.
- EPICS software has a home here: <https://epics-controls.org/>, and the technical documentation for the XIA Saturn driver for EPICS, by Mark Rivers at U. Chicago is here: <https://www.physics.brocku.ca/Courses/3P91/References/MCA/>.

Experiment 5

Electron Diffraction

Powder crystalline samples produce iconcentric-ring diffraction patterns that can be used to characterize the structure of the material. Electron diffraction, in particular, uses the wavelength that is well-suited to the analysis of the crystal structure of metals. In this experiment you will measure the de Broglie wavelength for fast moving electrons, directly demonstrating both the wave-particle duality and its practical use in the analysis of crystal structures of solid-state materials.

5.1 Introduction

In 1924, de Broglie proposed the hypothesis of wave-particle duality, associating with each particle a wave, the de Broglie wave, whose wavelength λ depended on the momentum p of the particle according to

$$\lambda = \frac{h}{p} \quad (5.1)$$

where h is the Planck's constant. The 1923-27 experiments of Davisson and Germer, in which electrons were scattered off a crystal of nickel and produced a diffraction pattern, were the first experimental confirmation of this hypothesis (the diffraction off a crystal came about quite accidentally, when a vacuum seal failed, and they heated their amorphous nickel target to get rid of the oxide film on its surface, which formed large nickel crystals). Independently, Thompson (1927) developed a scheme for firing the electrons through metal films, which is what is used in the apparatus for this experiment. Either method allows one to measure the de Broglie wavelength of fast moving electrons, and show that it is related to its momentum according to Eq. 5.1.

Scattering electrons through a metal film

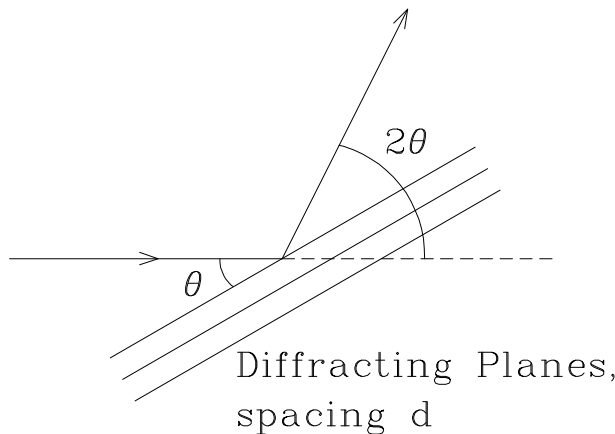


Figure 5.1: A schematic illustration of the formation of diffraction peaks in electron scattering.

If an electron leaves a cathode with zero velocity, then its kinetic energy after traversing an accelerating potential V is given by:

$$\frac{1}{2}mv^2 = eV \quad (5.2)$$

where m is the electron mass, v is its speed after traversing the potential V , and e is its charge. The momentum p of the electron is then given by

$$p = mv = \sqrt{2meV}$$

and its de Broglie wavelength

$$\lambda = \frac{h}{\sqrt{2meV}}. \quad (5.3)$$

If this electron strikes a crystal, its de Broglie wave will be diffracted by the 3-dimensional periodic

structure of the crystal. The electron will pass through the crystal only in those directions in which the de Broglie wave is diffracted strongly by the crystal. These directions are given by Bragg's Law:

$$2d \sin \theta = n\lambda \quad (5.4)$$

Therefore, if we know the d -values for a crystal (and we can calculate these if the crystal structure is known), then the wavelength λ can be found by measuring the directions (2θ) in which the waves are strongly diffracted, as illustrated schematically in Fig. 5.1.

Powder samples

Consider now the situation where a parallel beam of waves is incident on many crystals at once, oriented randomly with respect to direction of the beam. In such a random aggregate of crystals (*i.e.*, a powder) there are always crystals with the same set of lattice planes in an orientation satisfying Bragg's Law. All these crystals will diffract the incident beam strongly over the same angle 2θ , while other directions will result in destructive interference. The result is a diffracted beam in the shape of a cone with top angle 4θ .

This is the powder method of diffraction (Cullity, Chapter 3, p.96) and is the technique used in this experiment to measure the wavelength λ . Our beam of electrons is incident on a polycrystalline foil of aluminum. The cones of diffracted electrons strike a fluorescent screen at a distance D , forming a set of fluorescent rings of radius r . It is evident that diffraction angle 2θ is given by

$$\tan 2\theta = \frac{r}{D}. \quad (5.5)$$

The Bragg's Law

$$2d \sin \theta = n\lambda \quad (5.6)$$

may then be rewritten as

$$2 \left(\frac{d}{n} \right) \sin \theta = \lambda. \quad (5.7)$$

In Eq. 5.4 we refer to θ as the direction of the n -th order beam diffracted from the set of atomic planes with spacing d . In the alternative formulation (Eq. 5.6) we may refer to θ as the direction of the first-order beam diffracted from a set of planes with spacing d/n . For cubic crystals the distance d between successive lattice planes in the set specified by the Miller indices hkl is

$$d = \frac{a}{\sqrt{h^2 + k^2 + \ell^2}} \quad (5.8)$$

where a is the unit cell side length. Hence we may write

$$\frac{d}{n} = \frac{a}{n\sqrt{h^2 + k^2 + \ell^2}} = \frac{a}{\sqrt{H^2 + K^2 + L^2}} \quad (5.9)$$

where $H = nh$, $K = nk$, $L = n\ell$ are the Miller indices of a set of planes with spacing d/n .

In the present experiment, the diffraction angles are sufficiently small that $\tan 2\theta \approx 2\theta$ and $\sin \theta \approx \theta$. Hence, combining Eqs. 5.6–5.7, and 5.9 gives an expression for the electron beam wavelength in terms of the radii of the diffraction rings on the fluorescent screen, namely

$$\lambda = \frac{a}{\sqrt{H^2 + K^2 + L^2}} \frac{r}{D}. \quad (5.10)$$

Finally, by equating the expression for the diffraction measurement of the electron beam wavelength (Eq. 5.10) to the de Broglie expression for the electron-beam wavelength written in terms of the electron tube accelerating voltage V (Eq. 5.3) one obtains

$$r = \sqrt{H^2 + K^2 + L^2} \left(\frac{D}{a} \frac{h}{\sqrt{2me}} \right) \frac{1}{\sqrt{V}} \quad (5.11)$$

Eq. 5.11 gives an explicit expression for the radii of a set of diffraction rings as a function of accelerating tube voltage and its validity rests on that of the de Broglie postulate.

5.2 The apparatus

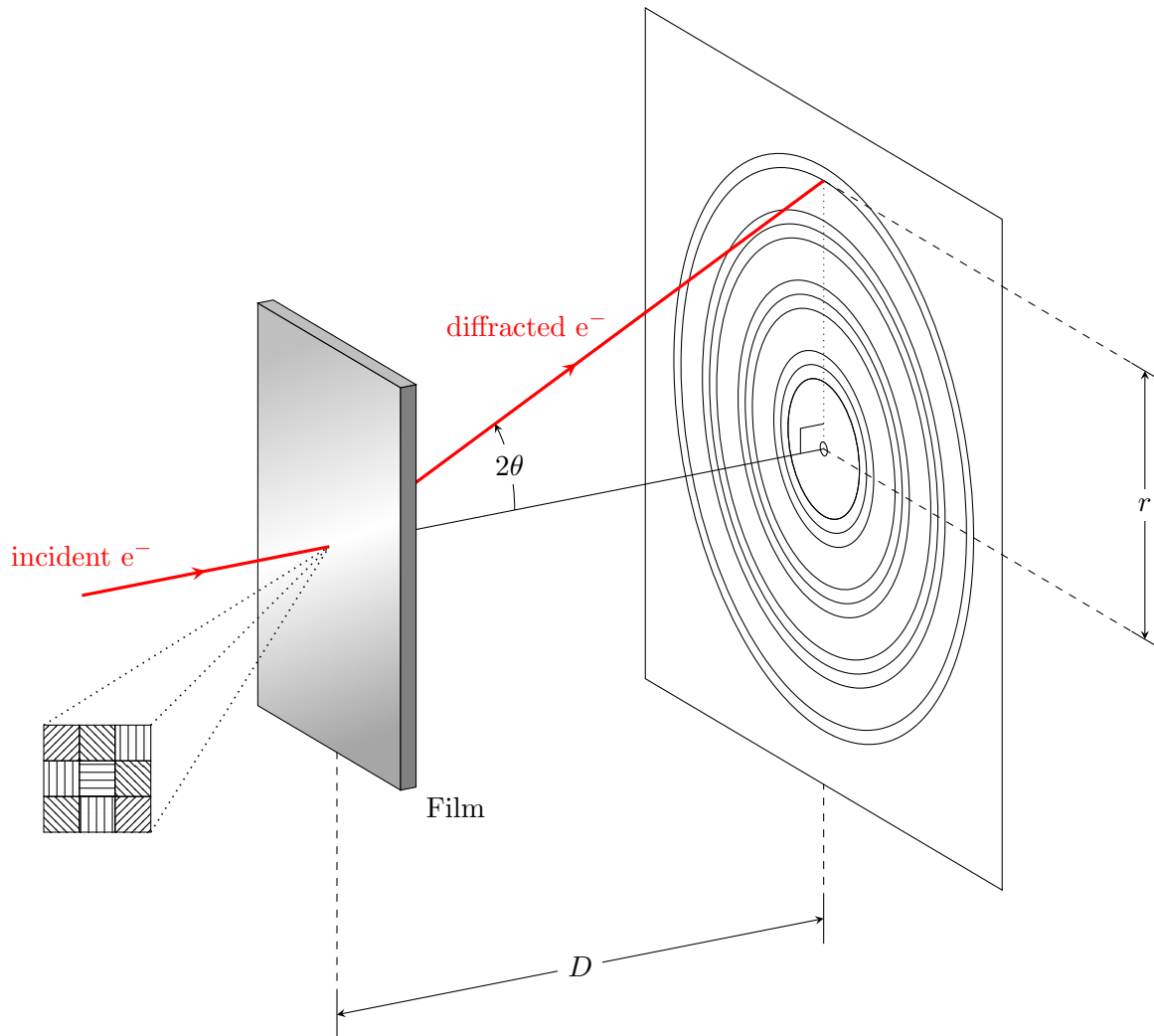


Figure 5.2: The experimental setup. Electrons are emitted from a hot cathode and accelerated through a strong electric field before striking a thin film of polycrystalline aluminium or gold. The film effectively presents itself as a collection of small crystals with their reflecting planes oriented in random directions (*i.e.* a ‘powder’). Many electrons pass through the target unaffected, forming a bright, central dot on the viewing screen a distance D away. Some electrons, however, will be incident at an angle meeting the Bragg condition and diffract through the film in a cone of angle 4θ , resulting in concentric rings of radius r on the viewing screen. This drawing in tikz is by C.Wilson.

The instrument is a modified cathode-ray oscilloscope with a variable accelerating potential V . The electron beam can be deflected with horizontal and vertical deflection plates till it strikes an Al foil in the tube. The diffraction pattern of the metal foil can be measured, using of of the commonly-used techniques:

- with a ruler directly on-screen;
- taping a transparent film over the screen and using a fine marker to record several points on each visible circle for late analysis; or
- using a DSLR camera to capture the images for later analysis.

The idea of analysing the digitized data is to overlay a series of concentric circles on the image and measure their diameters as precisely as possible. In practice, at least 4–8 points per circle need to be marked and digitized by hand, or a suitable fit algorithm to the spatial distribution of the image intensity needs to be employed.

There are two instruments available in the lab, the 2639 Electron Diffraction Tube by the Welch Scientific Company (Al foil as the target), and the LEAI-62 electron diffraction apparatus by Lambda Scientific (Au foil as the target). Both share the same basic design principles, with the Welch instrument having a unique feature of having a small piece of crystalline graphite embedded in the Al foil, in a slightly off-center location. It is there to demonstrate the differences in the diffraction patterns produced by powders (circles) and crystals (discrete Laue spots, of high symmetry determined by the crystalline structure). Feel free to use one or both of the instruments, and to compare, time permitting, the results. The distances between the metal foil and the screen inside the vacuum tube are fixed, and are indicated on the outside of each apparatus. For the Welch instrument it is $D = 18.2 \pm 0.2$ cm, and for the Lambda apparatus, $D = 25.3 \pm 0.3$ cm.

5.3 Measurement checklist

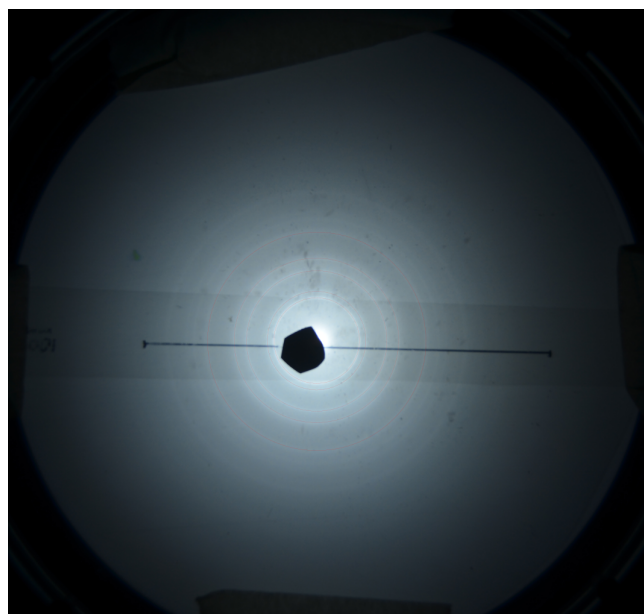


Figure 5.3: A typical diffraction pattern observed with the Welch apparatus. The black line is a scale used to convert the pixel measurements into centimeters.

To perform the experiment:

1. Review the detailed description in the manuals (see the References section below).
 2. Turn the device on and slowly increase the voltage up to 9,000V. Note: turn the voltage knob and the intensity knob down to zero before powering off the apparatus; make sure they are at zero before powering it on.
 3. Find a clean powder diffraction pattern (rings) by adjusting the vertical and horizontal deflection knobs. A “good” spot corresponds to a polycrystalline region of the foil; over the years, some spots were heated by overly intense electron beams and recrystallized, so they no longer act as “powder” regions.
- CAUTION:** Do not exceed $5 \mu\text{A}$ beam current.
4. Set the desired intensity ($4\mu\text{A}$ or so works well) and focus the beam so that the center point is as symmetric (round) as possible.

5. Place a transparent film (cut it roughly to the shape of the screen) over the diffraction pattern and fix it there using masking tape. Before taping the transparency write the voltage, intensity and your name on the transparency. A small piece of electrician’s black tape placed over the bright center spot will help to see the faint outer rings. A typical pattern as observed in the Welch apparatus is shown in Fig. 5.3.
6. Make five or more diameter measurements of each ring starting at the 1st order. For each measurement draw two dots on the ring located opposite each other. The shape of the rings may be slightly distorted, and this strategy helps to account for that. You may skip over some orders if the rings

are too close together, be sure to make note of the order of the rings you do record (e.g. 1,2,4,6...) directly on the transparency.

7. Remove the transparency and measure the diameter of the rings using the calipers.
8. Optionally you may scan your transparency and use some computer-based method of drawing a circle that passes through each set of 10 (or more) dots and recording its diameter. If you are planning to use this method, drawing a precise perpendicular pair of xy-axes on the transparency before scanning it might prove useful.
9. Repeat for other values of the accelerating voltage. It is best to start from the highest end where the diffraction spots are the brightest, then lower the voltage systematically, until the diffraction spots are no longer visible. Use 5–9 kV range of accelerating voltages for the Welch apparatus, and 6–14 kV for the Lambda apparatus.
10. *Optional:* On the Welch apparatus, locate the small (poly-)crystal of pyrolytic graphite (a bit above and to the left of the center of the screen) and record its diffraction pattern for at least two different voltage values. Use the data to characterize the lattice constant of pyrolytic graphite. Since this is a poly-crystal (a cluster of a few small crystals), small adjustments to the beam position might make a big difference to the sharpness of the Laue diffraction spots.

Alternative methods of data acquisition could be considered. A DSLR (Nikon 5100) is available in the lab, and so the patterns for each chosen voltage could be recorded instantly, and the measurements analyzed using a ruler on a printout, or a computer program that would fit the observed intensity patterns to a set of concentric rings. Care should be taken to align the camera's optical axis perpendicular to the viewing screen. Set the camera to a manual exposure mode and try a variety of exposure times. Sometimes overexposing (and washing out) the brightest ring may reveal additional details on the faint ones. Automatic exposure will offer a compromise that may not reveal either very well. A typical photograph obtained using the Lambda apparatus is shown in Fig. 5.4.

To place a convenient reference scale on the image, you can pre-draw a line segment of known length (say, 10.0 cm) on the screen or measure precisely (using calipers) the size of the decorative ring on the front of the apparatus, visible as the outermost ring in Fig. 5.4.

A note of caution: avoid the use of wide-angle lenses, typical of smartphones and other hand-held devices as they may provide a significant radial non-linearity. To minimize distortions, set the zoom on the DSLR lens to 50mm equivalent (roughly the optical power of the human eye; photography lenses are often optimized for this focal distance). For DSLR this typically means around $50\text{mm}/1.5 \approx 35\text{mm}$.

The method of spiral powder overlays (see the References section) may prove particularly helpful, or a custom digitization and fitting program or script could be employed.

From the data calculate average values of r for each ring, at each value of V . The value of a for aluminum is $a = 4.0495 \text{ \AA}$, for gold $a = 4.0782 \text{ \AA}$ (data from the Online Periodic Table). Verify Eq. 5.11.

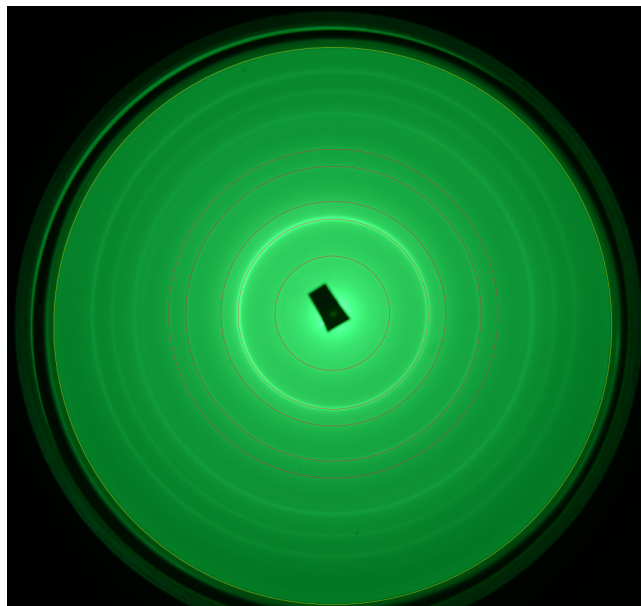


Figure 5.4: A typical diffraction pattern observed with the Lambda apparatus. The red circles have been superimposed using *inkscape* in order to measure the sizes of the diffraction rings.

References

Note that some of the links below require the class password for access.

- Davisson, C.; Germer, L. H. (1927). The Scattering of Electrons by a Single Crystal of Nickel. *Nature*, **119** (2998):558. <https://doi.org/10.1038/119558a0>.
- Thomson, G. P. (1927). Diffraction of Cathode Rays by a Thin Film. *Nature*, **119** (3007):890. <https://doi.org/10.1038/119890a0>.
- B.D.Cullity. Elements of X-ray Diffraction. Addison Wesley Mass. 1978 ISBN 0-201-01174-3. Available online at <https://pubs.acs.org/doi/abs/10.1021/ed034pA178>.
- N. Ashcroft and D. Mermin, Solid State Physics. Chapters 4 through 7 lay out the issues of crystallography and diffraction. See relevant excerpts:
 - From Ch.4: Crystal Lattices
 - From Ch.5: Lattice Planes and Miller indices
 - From Ch.6: Bragg and Laue Diffraction
- C. Kittel, Introduction to Solid State Physics. Chapter 1 is an introduction to crystal structure. Chapter 2 starts from diffraction and builds from there.
- Electron Diffraction Tube, instructions for catalog No.2639. The Welch Scientific Company.
- Cat.No.2639 Electron Diffraction Tube and Cat.No.2639A Power Supply, instructions for assembly. The Welch Scientific Company.
- LEAI-62 electron diffraction apparatus by Lambda Scientific (product brochure; a local copy).
- Spiral powder overlays are a novel way of analysing powder diffraction patterns, especially well-suited to electron diffraction.
- Electron Diffraction, an online book chapter.
- “Lattice Constants of the Elements.” Online Periodic Table. Accessed February 22, 2021. <https://periodictable.com/Properties/A/LatticeConstants.html>.
- WebPlotDigitizer tool may prove helpful. Our Linux workstations also have quite a number of powerful graphics tools installed (*xsane* scanning tool, *engauge* image digitizer, *inkscape* drawing program, *etc.*).

Experiment 6

The photoelectric effect

In this experiment we will determine the Planck's constant through photoelectric effect. Explaining the somewhat puzzling result — the stopping potential measured as the voltage produced by a photocell depends on the wavelength and, therefore, on the energy of the incident photons, but not in the intensity of the incident light — led to the beginnings of quantum physics. The experiment yields an excellent estimate of the Planck's constant.

6.1 Introduction

Photoelectric effect has a place of pride in the history of experimental Physics as one of the watershed experiments that led to the development of Quantum Mechanics. It is also what Albert Einstein got his Nobel Prize for. Since the apparatus is relatively simple, almost every undergraduate Physics major runs into this experiment at some point, and the web is full of reports of mostly poor quality. However, when the experiment is done well, it is a very reliable way of measuring the Planck constant, $h = 6.62607015 \times 10^{-34}$ Js (as established at the General Conference on Weights and Measures in 2018).

The Einstein photoelectric equation relates the kinetic energy K of the emitted electron to the frequency of the radiation falling on the emitter and the energy required to extract the electron from the material

$$K = h\nu - W_s = h\nu - eV, \quad (6.1)$$

where the extraction energy W_s , known as the work function of the material, is written as the product of the magnitude of the electron charge e and a retarding electric potential V . Electrons will be emitted only if $h\nu > eV$.

If the emitter is used as the cathode of a vacuum cell and connected to the other electrode, or anode, a current will exist in the circuit as long as light of sufficiently short wavelength falls on the cathode. If a retarding potential is applied between anode and cathode by an external source, the current will be reduced. The current will be zero if the retarding potential is set at the value $V_0 = h\nu/e$. In the experiment you will measure the retarding potential required to stop the photoelectric current as a function of frequency, or reciprocal wavelength: $c = \nu\lambda$ and therefore, $\nu = c/\lambda$ where c is the speed of light. A value of h will be determined from the graph of the “stopping” potential V_0 as a function of ν .

6.2 The apparatus

There are two versions of the apparatus available in the lab. One is a modified version of the LEAI-51 “Plancks Constant Apparatus” from Lambda Scientific (the ‘Lambda apparatus’, shown in Fig. 6.1), and another is custom-built and uses a research-grade Heathkit 619 electrometer (the ‘Heathkit apparatus’). There are subtle differences between the two setups, but the basic principle is the same: a monochromatic light shines on a photocell and the voltage required to stop the photocurrent is measured. In both setups, the source of monochromatic light is the mercury (Hg) discharge lamp with a dedicated power supply. This is potentially a dangerous device!

CAUTION: *Do not look into the Hg lamp, prolonged exposure can damage your eyesight. The power supply is a source of high voltage, do not touch the contacts when the power supply is on. Avoid quickly power-cycling the lamp: after it is turned off, it must cool down for at least 20 mins before you may turn it back on.*

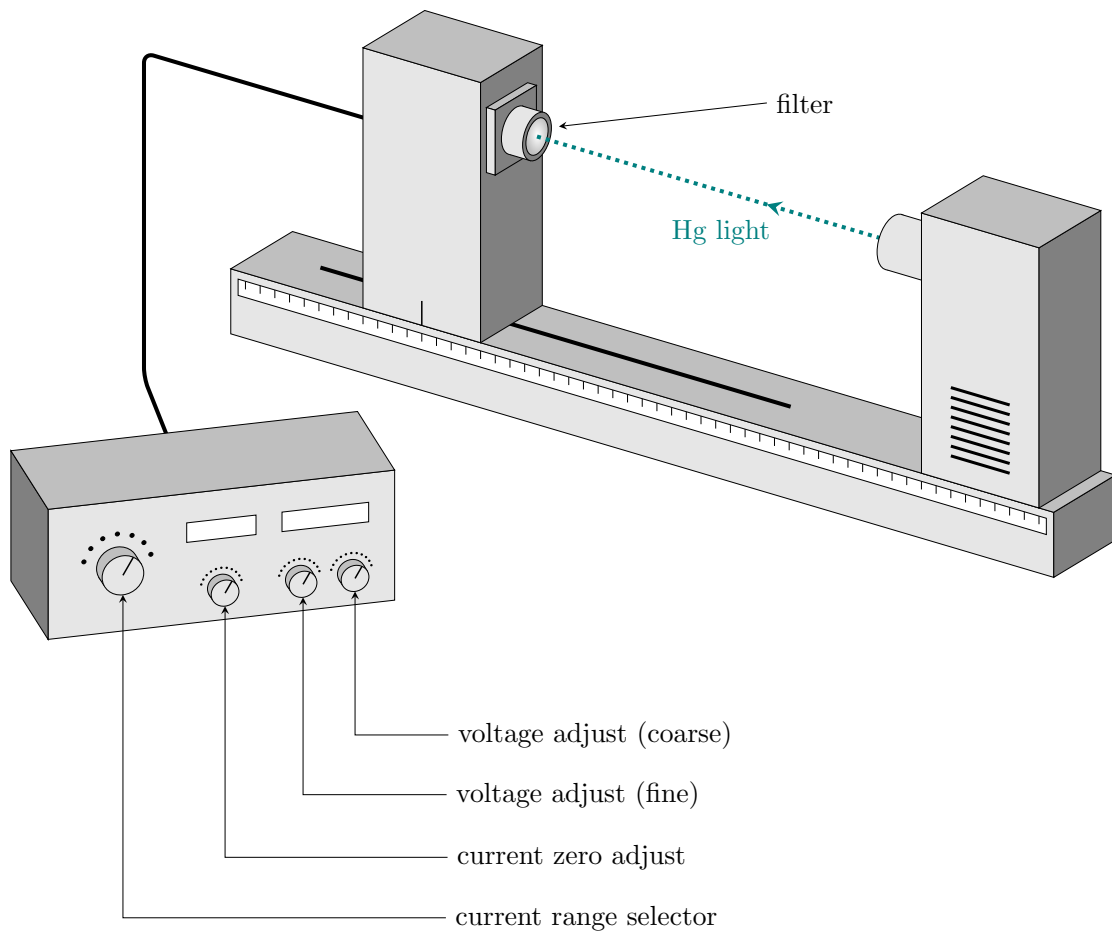


Figure 6.1: The LEAI-51 “Plancks Constant Apparatus” from Lambda Scientific. The photocell is on the left and the Hg source on the right. The photocell position can be adjusted by sliding the photocell enclosure along the track, its position monitored on the scale on the side of the track. An opening on the front of the photocell enclosure offers a snug fit to the interchangeable monochromatic filters. This drawing in tikz is by C.Wilson.

Table 6.1: Wavelengths (in air) of some of the strong lines of mercury (Hg) and the matching bandpass filters. Hg data from the National Institute of Standards and Technology (NIST); filter calibration data from Newport. For the 577-nm filter only the nominal values are available.

Hg lines		Available filters	
intensity (relative)	λ , nm	center λ , nm	1/2-power width, nm
600	365.0153	365.15	11.30
1000	398.3931	405.49	11.10
400	404.6563	405.49	11.10
1000	435.8328	435.35	9.70
500	546.0735	546.90	9.40
50	576.9598	577	10
60	579.0663	577	10
25	708.190	701.40	23.6

The mercury lamp needs to warm up, its output may be unstable during the first 10-15 mins. Make sure you turn it on and give it time to warm up before recording any measurements.

The mercury emission spectrum has a number of well-known lines, as seen in Table 6.1 where some strong lines are listed. A series of high-quality narrow-band filters are provided. These filters are extremely delicate and their optical surfaces, front and back, must not be touched by hand, or wiped with cloth. Each filter is mounted in a ring that can be safely handled and inserted into the opening in front of the photocell; they fit both the Lambda and the Keithley setups. Whenever not in use, they must be placed in their storage slots, and the lid of the box replaced.

The filters typically have the bandwidth of $\lesssim 10$ nm (see the calibration data for each filter, provided at the apparatus) and so select just one of the Hg lines at a time. The filters fit snugly into the openings in front of the photocell and this helps to reduce the amount of stray light reaching it, but it is best to conduct the experiment in a darkened room. The photocell has a potassium cathode and a ring anode (see Fig. 6.2) arranged so that the light can reach the cathode without striking the anode and causing the emission of electrons from the anode material, or from small amounts of potassium unintentionally deposited on the anode in the manufacturing of the cell. The photocell is mounted in its enclosure in such a way that the light enters through the middle in the ring and illuminates only the cathode.



Figure 6.2: An LD Didactic photocell, type 558 77. The potassium coating on the back surface of the cell is the cathode, and the wire ring suspended above it is the anode.

To adjust the intensity of the incident light, the distance between the lamp and the photocell can be varied, in both setups.

In the Lambda apparatus, the voltage is adjusted systematically, and the resulting current is measured, with readings displayed on the front panel of the LEAI-51 control box (see Fig. 6.1). With the incident Hg light blocked, the ammeter display can be zeroed with the ‘current zero’ knob. This compensates for the offset due to the dark current that flows when there is no light falling on the cathode in the photocell. The applied voltage is set with the ‘voltage adjust’ knobs. A good strategy is to explore the entire range of voltages, from -2 V to 30 V, in coarse steps, to get the overall feel for the range of responses, and then “zoom in” to the range of particular interest where non-linear changes in photocurrent occur, -2 V to +2 V. A typical set of results one might see is presented in Fig. 6.3. For retarding voltages that exceed V_0 , the photocur-

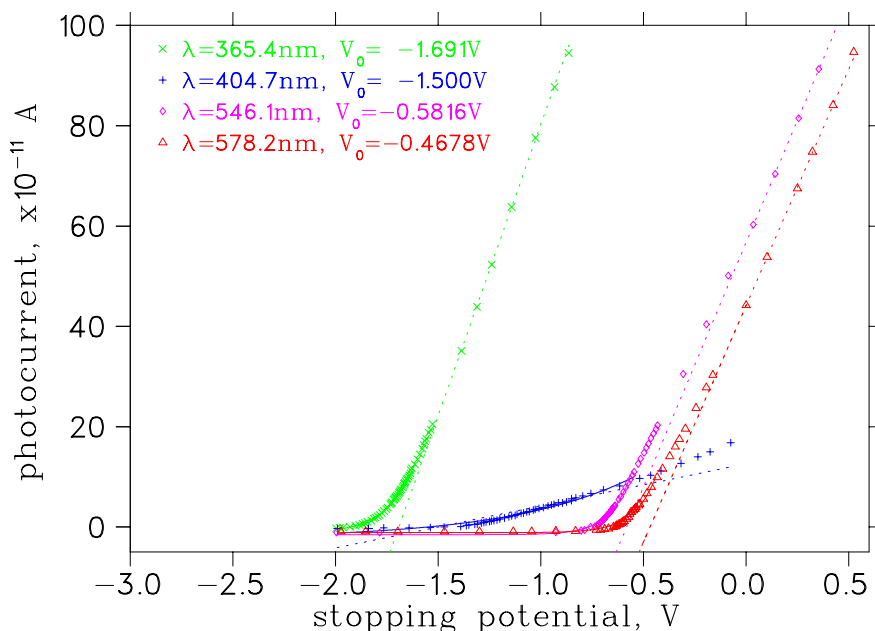


Figure 6.3: A set of measurements for four different bandpass filters, obtained on the Lambda apparatus. The stopping potential value can be obtained by a linear fit and extrapolation to zero photocurrent (the x -intercept, dotted lines) or by a fit to a Shockleys diode equation, for $I \leq 8 \times 10^{-11}$ A (solid lines).

rent is seen to be essentially zero, since the dark-current and contact-EMF were compensated for by the current zero adjustment, so the stopping potential value can be obtained by a linear fit and extrapolation to zero photocurrent.

In the Keithley apparatus the (same type of) cell is connected to a small low-leakage capacitor that gets charged by the photocurrent. As the capacitor charges, the counter voltage between the capacitor plates rises, the photo current is reduced, and eventually the voltage across the capacitor reaches a steady value. This value is the stopping potential (plus any contact EMFs arising from the connections between circuit elements, plus the offset due to the dark current). The offset voltages are unknown, but since data analysis involves fitting to a *slope* of the $V(\nu)$ dependence, these offsets do not affect the result, as long as they do not depend on wavelength and intensity (which they may, unfortunately).

The steady potential reached by the capacitor is measured by an electrometer rather than a voltmeter. The input impedance of the electrometer is so high that it does not provide any significant current drain of the charge of the capacitor. (This is not the case for everyday voltmeters, such as the one built into the Lambda control box). The current generated by a photocell is quite small, so it may take a few minutes for the voltage on the capacitor to reach its steady value. The capacitor must be discharged between measurements; the ‘zero check’ on the electrometer serves this purpose.

Fig. 6.4 shows a typical data set, and the resulting data fits, performed in two different ways: as an intersection of two straight line segments, one for the high enough counter voltages that the photocurrent is essentially constant, and one from the linear region of I vs. V dependence; the two segments intersect at V_0 . The second way is to fit all data (above zero current) to an exponential function, but allow an additional parameter of a vertical offset, to account for the offset voltages, the so-called Shockleys diode equation (see LD Physics Leaflet P6.1.4.4 for the details of this method). You may want to perform both forms of data analysis and to compare the results. The third line in Fig. 6.4 is the result of a direct measurement of stopping voltage using Keithley electrometer.

Make a graph of stopping potential V_0 as a function of reciprocal wavelength (or ν) and determine the Planck’s constant and the apparent work function of potassium.

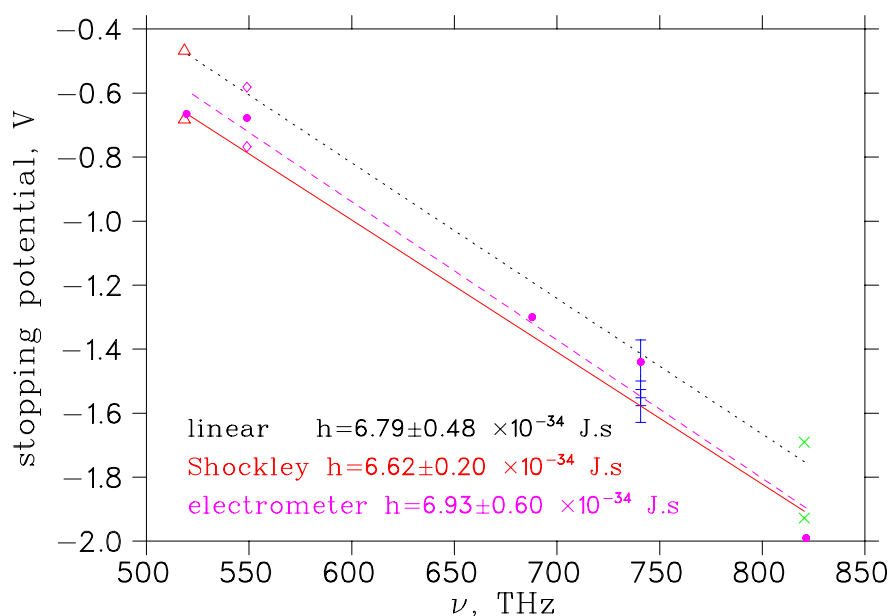


Figure 6.4: The results from the fits of Fig. 6.3 exhibit an approximately linear dependence on $\nu = c/\lambda$, from the slope of which h can be calculated, using a linear extrapolation (dotted line) or a fit to a Shockleys diode equation (solid line). The points are colour-coded to match Fig. 6.3. In addition, a set of direct measurements of the stopping potential V_0 obtained on the Keithley electrometer is presented (magenta circles, dashed line). Linear fits reveal the relationship $V_0(\nu) = h\nu/e$, from which h can be determined.

6.3 Measurement checklist

Review this manual, and the reference materials provided, to develop your own checklist before coming to the lab. Be sure to include it in your lab report, and comment on how well it worked. Devise a plan to explore the way the photocurrent depends both on the wavelength and on the intensity of incoming light. Determine Planck's constant.

References

Note that some of the links below require the class password for access.

- Resolutions of the 26th CGPM. Bureau International des Poids et Mesures (BIPM). 2018-11-16. <https://www.bipm.org/utis/common/pdf/CGPM-2018/26th-CGPM-Resolutions.pdf>. Retrieved 2021-02-22.
- LEAI-51 Apparatus for Determining Planck's Constant. Lambda Scientific Systems, Miami, FL. https://www.physics.brocku.ca/Courses/3P91/References/Planck/LEAI-51_Manual.pdf
- Determining Planck's constant: Counter voltage method. Leybold Physics Leaflets, P6.1.4.4. LD Didactic GmbH. Hürth, Germany. https://www.physics.brocku.ca/Courses/3P91/References/Planck/p6144_e.pdf.
- Photo cell for determining Plancks constant Photocell. Instruction Sheet 558 77. Leybold Didactic GmbH. Hürth, Germany. <https://www.physics.brocku.ca/Courses/3P91/References/Planck/55877e.pdf>.

Experiment 7

Blackbody radiation spectra

7.1 Introduction

The constant $h = 6.62559 \times 10^{-34} \text{Js}$ was introduced by Planck in 1900 to provide the first satisfactory theoretical basis for the temperature and wavelength dependence of the radiation from a black body. An idealized non-reflecting blackbody absorbs all the radiation that falls upon it, while the rate of all its energy emissions, summed over all wavelengths, is $\propto T^4$ where T is the thermodynamic temperature. Since there is no reflection off an ideal blackbody, the emitted spectrum, *i.e.* the distribution of the radiation intensity as a function of wavelength, is due to emission only. The radiative intensity depends on T , with a maximum in the emission versus wavelength curve such that the product of the characteristic wavelength of the maximum emission varies inversely with temperature, shifting to lower wavelengths (*i.e.* to higher frequencies) with increasing temperature. These relations are known as Stefan's Law and Wien's Law, respectively. In 1893, W.Wien showed from thermodynamic considerations that the form of the radiation curve was given by

$$E_\lambda = \frac{1}{\lambda^5} \times f\left(\frac{1}{\lambda T}\right) \quad (7.1)$$

where E_λ is the energy emitted in range $d\lambda$ centered at wavelength λ , and f is some function to be determined. The experimental data were obtained by W.Coblentz in 1914–16, who measured the emissions from a small aperture in a fully enclosed body (a metallic cylinder) with walls maintained at a constant temperature, which is a good approximation of a perfect blackbody because radiation that enters the hole from outside has an exceedingly small chance to escape before it is absorbed at the walls of the cavity (see A.C.Parr's article). The rate of emission is independent of the material that forms the walls of such a cavity. At the temperatures available in the laboratory the shortest wavelength radiation of measurable intensity is in the near-ultraviolet.

In 1900, Planck introduced the assumption that each mode of vibration of frequency ν ($\nu = c/\lambda$) of the electromagnetic field in the cavity could change its energy by a definite amount $h\nu$ (where h was a constant to be determined) rather than by continuously variable amounts. He was then able to derive the explicit form of the radiation curve and to show that Stefan's Law and the Wien Law followed from his form. Planck's formula for the power radiated by a black body at wavelength and temperature T is

$$\rho(\lambda, T) = \frac{2hc^2}{\lambda^5} \frac{1}{e^{hc/\lambda k_B T} - 1} \quad (7.2)$$

where the spectral radiance $\rho(\lambda, T)$ is the power (energy per second) radiated per solid angle and per unit area normal to the propagation, at frequency λ and temperature T , k_B is Boltzmann constant and c is the velocity of light. The form of the Planck's radiation curve is shown in Figure 7.1. The form determined by Coblentz matches the predictions of Planck's theory and his data yielded the value of h within 0.8% of the correct value. Planck's assumption was the first use of the idea of quantization in the radiation field and, later, in the interaction of radiation with atoms.

If a body is not a black body radiator, so that it does not absorb all radiation that falls upon it, the power radiated is less than the amount predicted by the Planck's formula, by a factor called emissivity, $0 < \varepsilon < 1$. However, if the emissivity ε coefficient at each wavelength is independent of the temperature, the emitted power is reduced by a constant factor for all temperatures. In addition, for the wavelength in

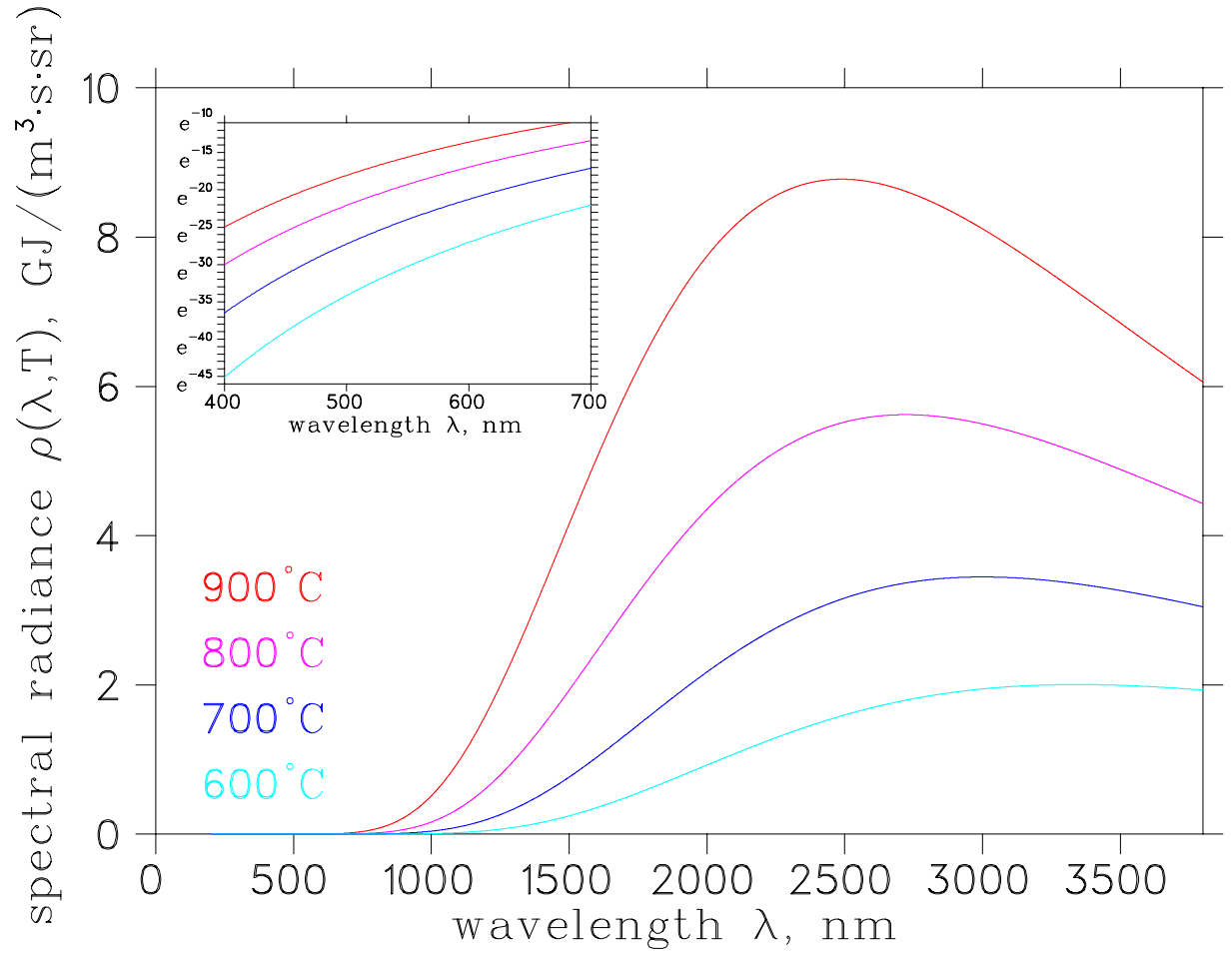


Figure 7.1: Temperature-dependent energy emission by a blackbody. The insert shows fragments of the same curves, on a logarithmic scale, in the range of visible light, 400–700nm. At those wavelengths, the spectral radiance is many orders of magnitude weaker than the peak intensity at each temperature, but it does exhibit a strong temperature dependence.

the visible, $\exp(hc/\lambda k_B T) \gg 1$. Thus

$$\rho(\lambda, T) \propto \exp\left(-\frac{hc}{\lambda k_B T}\right), \quad (7.3)$$

and a graph of $\ln \rho$ versus $1/T$ should be a straight line of slope $-hc/\lambda k_B T$. Using independently known values of c and k , a value for h can be obtained.

If the Planck's constant is known, one can use measurements of radiance performed at multiple wavelengths to estimate the temperature from the spectral radiance, using the so-called “two-colour method” used in various pyrometric instruments:

$$\frac{\rho_1}{\rho_2} = \frac{\varepsilon_1}{\varepsilon_2} \times \left(\frac{\lambda_2}{\lambda_1}\right)^5 \times \frac{e^{-hc/\lambda_1 k_B T}}{e^{-hc/\lambda_2 k_B T}} \quad (7.4)$$

which can be rewritten as

$$T = \frac{hc/k_B(1/\lambda_2 - 1/\lambda_1)}{\ln(\rho_1/\rho_2) + \ln(\varepsilon_2/\varepsilon_1) + 5 \ln(\lambda_1/\lambda_2)}, \quad (7.5)$$

where the ratio of two emissivities $\varepsilon_1/\varepsilon_2 \simeq 1$ if the two wavelengths $\lambda_{1,2}$ are chosen sufficiently close to each other which simplifies the calculations. Fitting to measurements at more than two wavelengths would allow for a simultaneous determination of both h and T .

7.2 The apparatus

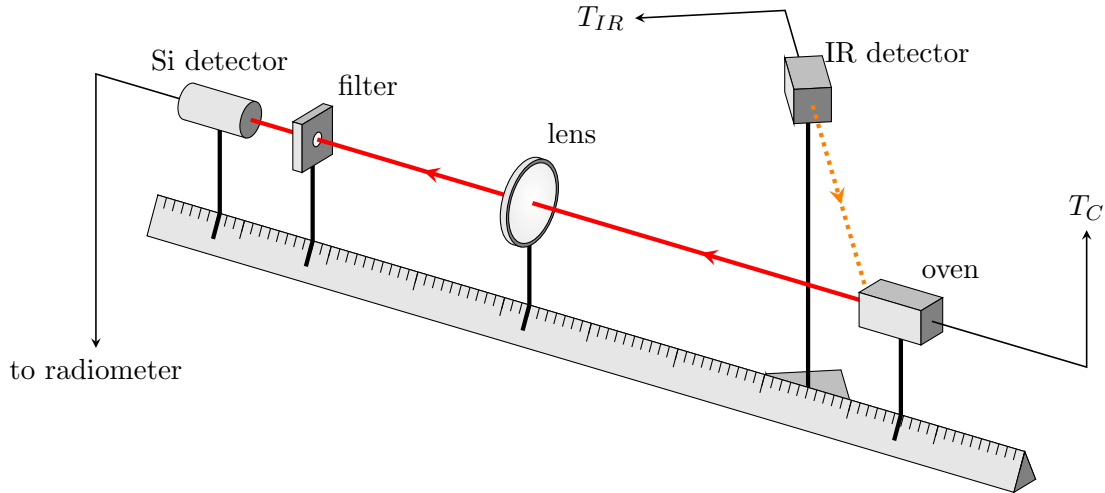


Figure 7.2: Experimental setup for determining Planck's constant from blackbody radiation. A hot MoSi_2 oven mounted on an optical bench emits thermal radiation through a narrow slit. The radiation passes through a lens focused on the Si detector. A narrow band-pass filter restricts the spectrum to be essentially monochromatic. The temperature of the oven is measured two different ways: using a Pt thermocouple (T_C) and with an infrared sensor (T_{IR}). Tikz figure by C.Wilson.

In the experiment we detect the intensity of the radiation reaching the Si photodetector attached to a radiometer. An oven cavity is a blackbody radiation source with a MoSi_2 heater element, controlled with a Variac. This oven can reach temperature as high as 1500°C . The temperature of the oven can be measured using several methods:

- directly using the S-type Pt thermocouple inside the oven;

- with an infrared pyrometer (by Omega Engineering) aimed and focused on the inside of the oven; the detector has a built-in aiming laser that can be used to align the detection direction exactly;
- using a glowing-filament radiometer, where an image of a glowing tungsten wire at a known temperature is superimposed and colour matched to the remote image of the inside of the oven.

In addition, the entire setup can be replaced with a USB spectrometer (by Ocean Optics), measuring the entire spectrum emitted from the oven. The spectrometer is uncalibrated and does not provide properly normalized spectrum (that could be used to fit to a Planck's distribution function to determine the temperature), but it does provide multiple regions in the visible where the dependence $\propto \exp(-hc/\lambda k_B T)$ can be observed, providing another way of analysing the data.

7.3 Measurement checklist

Review this manual, and the reference materials provided, to develop your own checklist before coming to the lab. Be sure to include it in your lab report, and comment on how well it worked. Devise a plan to explore several ways of measuring the temperature and discuss their relative merit. Determine Planck's constant.

References

Note that some of the links below require the class password for access.

- A.C.Parr. Determination of the Constants of Total Radiation From a Black Body. NIST. <https://nvlpubs.nist.gov/nistpubs/sp958-lide/007-009.pdf>. Retrieved 2021-03-01.
- M.Virgo, K.J.Quigley, S.Chemerisov and G.F.Vandergrift. Low-Cost, High-Performance Alternatives for Target Temperature Monitoring Using the Near-Infrared Spectrum. ANL/NE-17/3. Nuclear Engineering Division, Argonne National Laboratory. 2017. <https://www.physics.brocku.ca/Courses/3P91/References/Planck/ANL-NE-17-3.pdf>
- R.A.Rossow. Blackbody temperature calculations from visible and near-IR spectra for gas-fired furnaces. PhD thesis. 2005. University of Missouri-Columbia. <https://www.physics.brocku.ca/Courses/3P91/References/Planck/Rossow2005.pdf>
- ILT1700 Research Radiometer. Instruction manual. International Light Technologies, Peabody, MA. 2007. Retrieved 2021-03-03. See especially Section 8. https://www.intl-lighttech.com/sites/default/files/pdf/manual/ILT1700_Manual.pdf
- Directions for No.8621, No.8622 and No.8623 Optical Pyrometers. Std. 1295. Leeds & Northrup Company. Philadelphia, PA. <https://www.physics.brocku.ca/Courses/3P91/References/Planck/Leeds%20%20Northrup-Optical%20Pyrometers%208621%208622%208623.pdf>
- iR2 Ultra High Performance 2-Color Fiber Optic Infrared Ratio Temperature Measurement & Control System. User's Manual. Omega Engineering, Inc. <https://www.physics.brocku.ca/Courses/3P91/References/Planck/M3752.pdf>
- USB2000 Miniature Fiber Optic Spectrometers and Accessories. Operating Manual and Users Guide. Ocean Optics Inc., Dunedin, FL. https://www.physics.brocku.ca/Courses/3P91/References/Planck/USB2000_Operating_Manual.pdf

Experiment 8

Raman spectroscopy

8.1 Introduction

Light interacting with matter can be reflected, absorbed, or scattered. Absorption happens when the energy of the incoming photon matches the difference in the energies of two quantum levels of the system. In Raman spectroscopy these quantum levels are vibrational (and sometimes, rotational) molecular modes. After absorbing the incident photon, the system can also emit a photon, resulting in scattering. When the wavelength of the emitted photon is the same as the incident wavelength, the process is called Rayleigh scattering, but it is also possible for the system to relax into a state different from the initial one, thus producing an emitted photon of a different wavelength. In this case of inelastic scattering, longer wavelengths correspond to photons shifted to lower energies compared to the incident photons, the so-called Stokes shift, and shorter wavelengths (emitted energies higher than incident energies) correspond to the anti-Stokes shift. The observed shifts are a direct measure of the vibrational (and sometimes, rotational) frequencies in the material which depend on the chemical bond structure and molecular symmetry. In this way, Raman spectroscopy provides a “fingerprint” to identify materials.

The history of the discovery of Raman scattering is fascinating, and involves a number of very human and not just purely scientific aspects: prejudice, nationalist pride, public relations management. Chandrasekhara Venkata Raman reported the effect in 1928 via a telegram to *Nature*, and a press conference to the newspapers on February 28, 1928, both rather unusual at the time. He then successfully lobbied for a Nobel prize, and solicited the support of A.Sommerfeld, N.Bohr and E.Rutherford. He was awarded the prize in 1930, an unusually short time after the discovery, reflecting a universal recognition of the importance of the technique. Today in India, February 28 is celebrated as a National Science Day. *The Quantum Indians*, a 2013 film by Raja Choudhury is recommended viewing.

8.2 The apparatus

Fig. 8.1 shows a schematic diagram of the Raman spectrometer. The light source is a 632.8-nm (red) He-Ne laser, and a number of lenses and mirrors are used to route the incident beam to the sample and to collect the scattered light onto a narrow-slit entry point of the spectrometer. The lenses are built into the frame of the apparatus and require a minimum of adjustment, but the role of the filters needs to be well understood. Filter F_1 is a band-pass filter with peak transmission close to the 632.8-nm wavelength of the laser; filter F_2 is a notch filter greatly suppressing the 632.8-nm line. When both filters are in place, the incident light is purely the main, 632.8-nm line of the He-Ne laser, and the scattered light is at wavelengths that are *not* 632.8-nm. This combination allows for the detection of only those wavelengths that are different from the incident laser light and thus represent the Raman-shifted wavelengths.

The diffraction grating can be rotated by a micrometer screw, and its reading corresponds approximately to the wavelength at the center of the camera view. For precise measurements, the spectrometer needs to be calibrated, for every position of the grating. He-Ne laser output is strongly dominated by the the main 632.8-nm line, but a number of much weaker He plasma lines are also present; this is helpful to obtain the precise calibration of the spectrometer in the region of interest, since these wavelengths are well known. It is best to rotate the grating to a position somewhere in the 654–660 nm, as this places the main line just outside the view of the camera. Even the residual shoulder intensity is quite strong, and the use of the filter F_2 is essential. However, for calibration purposes filter F_1 should be removed. This allows the

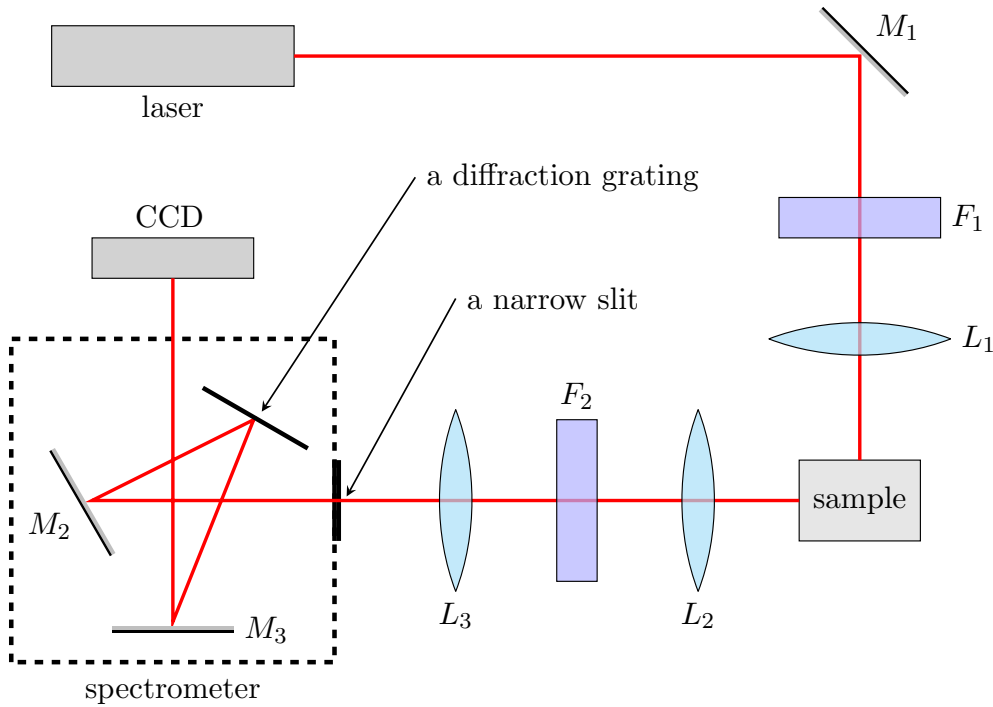


Figure 8.1: Schematic diagram of the Raman spectrometer. A 632.8-nm (red) He-Ne laser beam is directed at a sample and the scattered light passes through a narrow (50-nm) slit onto a diffraction grating before being detected by a CCD camera. A micrometer (not shown) can adjust the angle of the diffraction grating, shifting the window of detectable wavelengths. Filter F_1 is a band-pass filter with peak transmission close to the 632.8-nm wavelength used; while filter F_2 is a notch filter greatly suppressing the 632.8-nm line. This combination allows for the detection of only those scattered wavelengths that are different from the incident, purely 632.8-nm laser light. When the plasma lines from the He-Ne laser need to be detected during the calibration stage, filter F_1 must be removed. Tikz figure by C.Wilson.

plasma lines to be transmitted to the sample. Using a small metallic mirror (at grazing incidence) as the sample allows these wavelengths to be captured and used for calibration. Fig. 8.2 shows the result of a 60-second data acquisition and the resulting calibration table, as obtained using the `Raman.tcl` control script. A 60-sec dark spectrum (with the spectrometer entry slit blocked) has been subtracted. A linear fit to the calibration dataset was performed and applied, as evidenced by the x -axis labelled in nm (prior to calibration the axis reads in pixels). A remnant of the strong main line, off to the left of the observed region, is visible as a “shoulder” at 640–645 nm. The calibration data set can be saved, and if the micrometer position has not changed, loaded into the software and re-applied. The CCD is kept at -20°C to reduce noise.

Solid samples are mounted using a small amount of silicone grease on the removable steel holders. A careful adjustment of the position of the spot where the laser light grazes the surface of the solid sample is required, so that the weak scattered light is focused precisely on the narrow slit of the spectrometer, and then the notch filter F_2 placed back in the path. Liquid samples fill a cuvette, with most of the laser light passing through the liquid, and the scattered light collected at right angle to the direction of the laser beam; alignment is less critical in this case. Fig. 8.3 shows the spectrum of a liquid sample of toluene, acquired for 240 s for both the raw and the dark (with entry slit blocked) spectra. The raw spectrum is difficult to distinguish from the background of the dark spectrum, but the point-by-point difference reveals a number of weak lines.

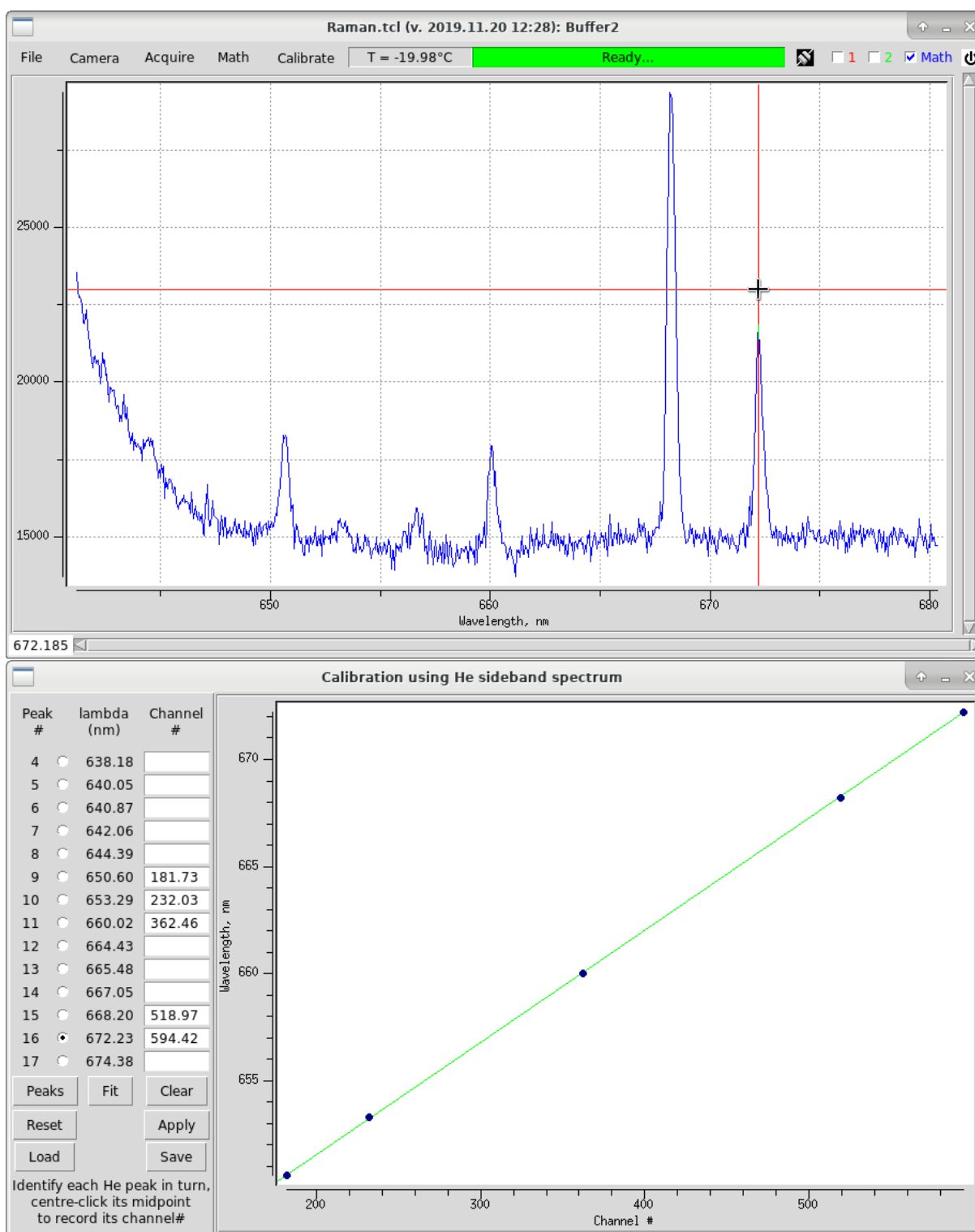


Figure 8.2: He plasma lines are used to obtain the calibration of the CCD camera.

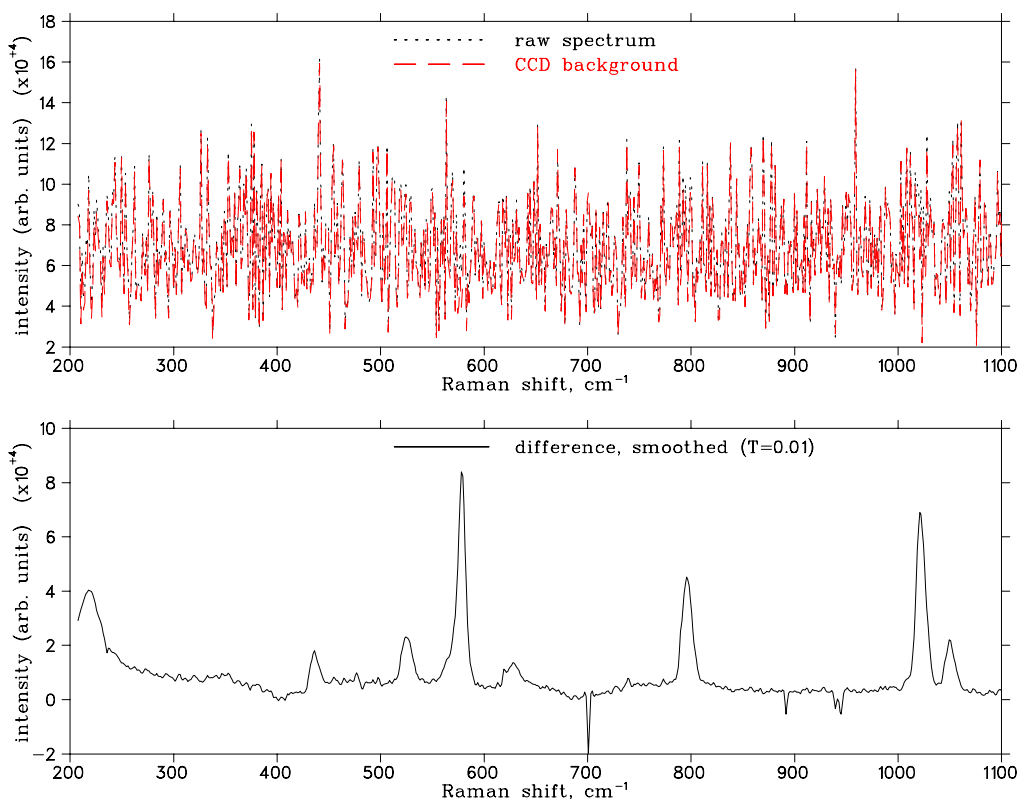


Figure 8.3: Raman spectrum of toluene.

8.3 Measurement checklist

Review this manual, and the reference materials provided, to develop your own checklist before coming to the lab. Be sure to include it in your lab report, and comment on how well it worked. Perform the spectrometer calibration using He plasma lines, then obtain spectra from several solid and liquid samples provided. Explain unusual features (*e.g.*, a sharp negative line near 700 cm^{-1} in Fig. 8.3).

References

Note that some of the links below require the class password for access.

- C.V. Raman, A new radiation. *Indian Journal of Physics*, **2**:387–398, 1928.
- *The Quantum Indians*, a film by Raja Choudhury. 2013. https://www.youtube.com/watch?v=7z9NUV_Yr0o, accessed 2021-03-08.
- Hecht, Eugene. Optics, 4th ed. Pearson Education Inc., San Francisco, 2002.
- Legacy product support from Diffraction Limited (formerly SBIG - Santa Barbara Instrumentation Group), makers of the CCD camera. <https://diffractionlimited.com/legacy-product-support/>
- Kestrel Spec software by Catalina Scientific: <https://www.catalinasci.com/kestrelspec.cfm>. A Mac version of an older manual: <https://www.physics.brocku.ca/Courses/3P91/References/Raman/KesST6m.pdf>. A self-explanatory tcl/tk interface by Phil Boseglav offers a more streamlined package, highly suitable for this experiment.